COMPOSITE PLASTER CEMENT-BASED ELECTROMAGNETIC WAVE ABSORBER

by

Johann Christiaan Pretorius

Submitted in partial fulfilment of the requirements for the degree

Master of Engineering (Electronic Engineering)

in the

Department of Electrical, Electronic and Computer Engineering
Faculty of Engineering, Built Environment and Information Technology
UNIVERSITY OF PRETORIA

July 2013

SUMMARY

COMPOSITE PLASTER CEMENT-BASED ELECTROMAGNETIC WAVE ABSORBER

by

Johann Christiaan Pretorius

Supervisor(s):	Prof. B.T.J. Maharaj
Department:	Electrical, Electronic and Computer Engineering
University:	University of Pretoria
Degree:	Master of Engineering (Electronic Engineering)
Keywords:	Electromagnetic waves, absorber, reflection loss, shielding effectiveness, propagation loss, building material, GSM frequency bands, wireless communications, WiFi, electromagnetic interference

The electromagnetic wave absorption characteristics of composite cement-based building material have attracted much interest in recent times. Researchers have mainly focused on the 2 GHz to 12 GHz frequency range. Mobile and wireless communication systems use frequencies from 800 MHz upwards. The determination of characteristics such as reflection loss, absorption, attenuation and shielding effectiveness are crucial in the evaluation and development of these materials for the building industry. Absorption is an indication of how much of the EMW energy enters the material. Attenuation indicates how much of the absorbed energy is converted into other forms of energy by the material. Shielding effectiveness (SE) is a combination of reflection loss, attenuation and multiple internal reflections and attenuations.

This research determined these characteristics by measuring the S11 and S21 parameters of the composite cement-based material in the GSM and WiFi frequency bands. The time

domain gating function of a vector network analyser is applied to measure the reflection from the material. The data was then used to obtain the reflection and absorption losses in the frequency bands. The transmission loss was measured by placing the sample in the propagation path between two antennas.

MnZn-ferrite and electrolytic manganese dioxide in powder form were evaluated as absorber material to increase the permeability of the cement-based material to improve absorption and attenuation capabilities to create a cost-effective practical electromagnetic wave absorber. The compound of the cement-based material was cement, sifted river sand and filler powder.

The results achieved in the research showed the uniqueness of electrolytic manganese dioxide as filler in composite cement based material for electromagnetic wave shielding effectiveness improvement. The combined measurement techniques used in this research were uniquely used to determine the required electromagnetic wave absorption characteristics and shielding effectiveness of 10 dB was measured in the GSM850 and GSM900 frequency bands.

OPSOMMING

SAAMGESTELDE PLEISTERSEMENT GEBASSEERDE ELEKTROMAGNETIESE GOLF ABSORBEERDER

deur

Johann Christiaan Pretorius

Studieleier(s):	Prof. B.T.J. Maharaj
Departement:	Elektriese, Elektroniese en Rekenaar-Ingenieurswese
Universiteit:	Universiteit van Pretoria
Graad:	Magister in Ingenieurswese (Elektroniese Ingenieurswese)
Sleutelwoorde:	Elektromagnetiese golwe, absorbeerder, weerkaatsings verlies, afskerm effektiwiteit, voortplantings verlies, boumateriaal, GSM frekwensiebande, koordlose komminikasie, WiFi, elektromagnetiese inmenging

Die Federale Kommunikasie Kommissie (FKK) het voorspel dat ’n spektrum-tekort in die nabye toekoms, onder die huidige regulatoriese omgewing, ondervind kan word. Hierdie dreigende spektrum-tekort is gedeeltelik as gevolg van die vinnig groei van aanvraag na draadlose dienste en van ondoeltreffende gebruik van die huidige gelisensieerde spektrum. ’n Nuwe paradigma met betrekking tot draadlose spektrumtoekenning, wat bekend staan as kognitiewe radio (KR), is voorgestel as ’n moontlike oplossing vir hierdie probleem.

Die doel van hierdie verhandeling is om navorsing op die gebied van KR te doen. Die navorsing sal bydra deur ’n ondersoek in te stel op die effek van ’n primêre gebruiker (PG) kanaalbesettingsmodel op die prestasie van ’n sekondêre gebruiker (SG) in ’n KR-netwerk. Die model is gebaseer op die aanname dat die PG-kanaalbesetting as ’n binêre proses beskryf kan word en ’n twee-toestand Verborge Markov-model (VMM) is dus vir hierdie ondersoek gekies. Tradisionele algoritmes vir die afrigting van die model is met sekere evolusionêre-gebaseerde opleidingalgoritmes in terme van hulle voorspelling van akkuraatheid en bere-

keningkompleksiteit vergelyk. Die prestasie van die model is belangrik omdat dit SGs ’n basis bied vir kanaalskakeling en toekomstige kanaaltoekennings.

’n Basis vir KR-simulasies is ontwikkel en die effek wat dié model op die kanaalskakeling het sowel as die bereikbare prestasie van ’n SG binne ’n KR-netwerk is deur die resultate geïllustreer. Prestasie met betrekking tot die haalbare deurvoer van SG data, PG-ontwrigtingkoers en die SG-kragverbruik, is vir beide teoretiese toetsdata asook die data wat verkry is deur werklike spektrummetings (geneem in Pretoria, Suid-Afrika) word geïllustreer. Die resultate wys dat daar ’n duidelike verband bestaan tussen die haalbare SG-deurset en die gemiddelde PU-ontwrigtingkoers. ’n Beduidende SG-prestasieverbetering is waargeneem wanneer voorspellingsmodellering gebruik word en dit is gevind dat die prestasie en kompleksiteit van die model beïnvloed word deur die algoritme wat gebruik word om dit op te lei. SG-prestasie word ook deur die lengte van die vinnige afmeting in tyd beïnvloed. Uitslae wat verkry is op grond van gemete besettingsdata is vergelykbaar met dié wat met teoretiese besettingsdata verkry is, met ’n gemiddelde gelykvormigheidstelling van 95% vir die voorspellingakkuraatheid, 90% vir die SG-deurset, 83% vir die SG-kragverbruik en 71% vir die PG-ontwrigtingskoers.

I dedicate this work to the Lord All Mighty.

ACKNOWLEDGEMENTS

I would like to thank the following people and organisations for their assistance in making this work possible:

- My family for their selfless support and encouragement.
- My supervisor, Prof B.T. Maharaj, for his provision and guidance.
- SAAB Grintek for making their equipment available for this research.

LIST OF ABBREVIATIONS

CB	Carbon black
CBCC	Cement-based composites
CW	Continuous wave
DC	Direct current
DSP	Densified small particles
DUT	Device under test
EMD	Electrolytic manganese dioxide
EMI	Electromagnetic interference
EMW	Electromagnetic wave
EPS	Expanded polystyrene
FSS	Frequancy selective surfaces
ICASA	Independant Communications Authority of South Africa
IF	Intermediate frequency
ISM	Industrial Scientific and Medical Bands
LOS	Line of sight
NRL	Naval Research Laboratory
PC	Personal computer
RF	Radio frequency
RX	Receiver
SE	Shielding effectiveness
SNR	Signal-to-noise ratio
TEM	Transverse electromagnetic wave
TLM	Transmission line modeling
TX	Transmitter
UP	University of Pretoria

UWB	Ultra-wide band
VNA	Vector network analyser
VSWR	Voltage standing wave ratio
WB	Wide band
WLAN	Wide band local area network
WAS	Broadband wireless access

LIST OF SYMBOLS

A	Attenuation
α	Attenuation constant
B	Magnetic flux density
β	Phase constant
C	Capacitance
D	Electric displacement
E	Electric field intensity/strength
G	Conductance
ε	Dielectric constant
Γ	Reflection coefficient
γ	Propagation constant
H	Magnetic field intensity/strength
I	Current
J	Electric current density
L	Inductance
M	Multiple internal reflection and attenuation loss
m	Magnetic moment
η	Intrinsic impedance in material
η_0	Intrinsic impedance in free space
ρ	Electric charge density
P	Power
R	Resistance
R	Reflection loss
s	Complex frequency
σ	Electric conductivity
σ_r	Electric conductivity relative to copper
S_{11}	Scattering parameter: input reflection coefficient
S_{21}	Scattering parameter: forward transmission coefficient

T	Transmission loss
μ	Initial magnetic permeability
μ_r	Relative magnetic permeability
V	Potential
υ	Velocity
ω	Radian frequency
x	Length
Y	Admittance
Z	Impedance
z	Thickness of material

LIST OF TABLES

LIST OF FIGURES

TABLE OF CONTENTS

CHAPTER 1

INTRODUCTION

1.1 MOTIVATION

The electromagnetic wave (EMW) absorption capability of composite cement-based material has attracted much attention from researchers in recent times. The continues exposure to EMW radiation has raised concern of potential health effects [4]. Accordingly researchers have adopted various methods to determine the absorption characteristics of such materials. It has been found that wireless communication and wireless networks are affected by the propagation characteristics of building materials, with cement-based material being one example. Knowledge of the absorption, attenuation and reflection ability of building materials allows for the proper implementation of indoor wireless communication and network systems. The accurate determination of these characteristics is of high importance for such implementations. Various methods have been reported in the literature to determine the characteristics of building material. Such knowledge also allows for the manipulation of the composition of the building material to achieve the required results for specific applications.

Absorption is an indication of how much EMW energy enters the material. Attenuation, on the other hand, indicates how much of the absorbed energy is converted into other forms of energy by the material. The most common method used to determine absorption is to measure the reflection loss S_{11} of the material by placing a conductive back plate behind

the device under test (DUT). This is done practically using a vector network analyser (VNA) and two horn antennae in an anechoic chamber [5], [6]. This experimental setup measures the total EMW energy attenuated by the material.

Shielding effectiveness (SE) is a combination of reflection loss and attenuation, as well as multiple internal reflections and attenuations [7]. SE can be measured by placing the DUT between two horn antennae and measuring the transmission loss (S_{21}) through the material [8]. This method gives an indication of the total shielding effect, but it does not reveal the actual attenuation of the EMW in the material.

In the literature and in various applications, different composite cement-based materials are used to absorb and attenuate EMW energy. For example, expanded polystyrene is added to a cement-based EMW absorber to improve its absorbing properties [6]. This method shows that the attenuation is mainly due to multiple internal reflections and scattering. SE of 6 to 16 dB in the 8 to 18 GHz frequency range has been reported in the literature. Further, carbon fillers [5] in the form of graphite and carbon black are used for shielding and absorption respectively. Moreover, SE of 5 to 15 dB is achieved in the 2 to 8 GHz frequency range with carbon black. It has also been found that ferrite and stainless steel powder can serve as a wooden building material for EMW absorption in indoor applications [9]. Absorption of above 10 dB is measured at frequencies above 2 GHz. However, the cost of these fillings is high and they are complicated to process. Research has mainly been concentrated on the 2 to 12 GHz frequency range.

Standard concrete walls of 300 mm thickness show an SE of 3 to 4 dB for frequencies between 500 MHz and 1.1 GHz [10]. However, this low level of SE can be increased by altering the composition of the structure in various ways as indicated above. Apart from the walls, there are also many apertures such as doors, windows, air-conditioning ducts and cable holes that are sources of EMW penetration. Accordingly, different aperture shapes have been modelled to determine SE in the GSM frequency bands [11]. SE variations of 1 to 5 dB were achieved by the apertures examined.

1.2 RESEARCH QUESTION

The interest shown by literature to material as absorber of EMW specially in building material, emphasises the need for suitable and cost effective building materials to improve the SE of building material and buildings. This quest is still to be successful for the different global conditions. In Africa and specifically in South Africa this need has not been investigated and fulfilled. The literature uses various methods of measuring SE to determine its effectiveness. An accurate method of measuring SE to manipulate the characteristics of composite building material is still a unanswered question. In this dissertation the research done to find solutions for the mentioned research questions is discussed.

1.3 RESEARCH OBJECTIVE

This study investigated the feasibility of using ferrimagnetic and magnetic material in a cement-based composite to develop an optimal EMW absorber building material for mobile and wireless communication system radiation in order to prevent EMW from entering or exiting a room or building. Various ratios of substances containing ferrite and magnetic material can be used to achieve effective attenuation of the EMW through the material. The South African manufactured magnetic powder MnO_4, known as electrolytic manganese dioxide (EMD), is investigated as an absorbing filler to improve the absorption and attenuation characteristics of cement-based composite building material for South African and African conditions. The absorber has to be cost-effective, decorative and practical for the use as a building material.

Various methods for measuring the SE characteristics of building material is investigated to suggest and confirm a more complete method than reported in the literature.

1.4 AUTHOR'S CONTRIBUTIONS AND OUTPUTS

In this research, the author reports on research findings to determine the exact absorption and attenuation capabilities of cement-based building material in mobile communications

and indoor wireless communication systems. The measurement techniques that are used determine and identify the absorption, attenuation and reflection loss components of the SE capabilities of the composite building material. The absorption is determined by using the gating function of a vector network analyser (VNA) measuring in the time domain to find S_{11}. The transmission coefficient is determined by measuring the S_{21} parameter and positioning the DUT in the EMW propagation path between the sending and receiving antennae. Consequently, the combination of the results of the two measurement methods enables one to determine the reflection, absorption and attenuation capabilities.

1.4.1 Research contribution

The author's main research contribution can be summarised as follows:

Combining the results of two measuring methods enabled the author to accurately characterise cement-based composite building material in terms of reflection loss, transmission loss, absorption and SE. The author also compared commonly used ferrimagnetic material MnZn-ferrite, with electrolytic manganese dioxide (EMD), as a filler for cement-based building material in terms of to improving the SE characteristics. It was found that, as a new magnetic filler, EMD is superior to MnZn-ferrite in terms of SE improvement.

1.4.1.1 Measurement system

To determine a complete measure of the SE, a combination of measurement systems was used to measure the reflection loss, transmission loss, absorption and attenuation of the building material. The measuring setup in Figure 3.6 was used to measure the S_{21} scattering parameter to find the SE. This setup was combined with the measurement of the S_{11} scattering parameter to find the reflection loss using only the transmitting (TX) antenna. The author combined the results of the two measurements to determine the absorption and attenuation by the material.

1.4.1.2 Plaster cement absorbing shield

Plaster cement, also referred to as cement mortar, is the material most widely used to finish off the concrete and brick walls of buildings. It is applied to the walls in a layer of between 15 mm and 25 mm in order to leave a smooth surface. Plaster cement has an SE of 2 to 4 dB for frequencies between 100 and 400 MHz [12]. An SE of less than 5 dB was measured between 1 and 6 GHz by [13]. In the 8.2 to 12.4 GHz frequency range, an SE of less than 3 dB was measured by [14].

The literature gives various techniques for improving the SE of a building or enclosure by [15], [12], [6], [16], [17], [18] and [19], as discussed in the literature study of this document. In this research the SE of plaster cement in the GSM bands and the WLAN band was measured and increased by adding ferrite and magnetic fillers. The author found that modifying plaster cement by adding a magnetic material to the composition of the cement-based material can improve its SE. This new composite plaster cement can then easily be applied to the surface of a concrete or brick wall to improve its SE. Normal plaster cement is prepared by mixing one part cement with six parts sifted river sand. The magnetic material is then added to the mixture by replacing a proportional amount of river sand with the magnetic material in powder form. For testing purposes, the composite plaster cement was moulded in tile format as shown in Figure 3.4.

1.4.2 Journal publications and conference papers

The following peer reviewed and accredited journal articles have been published by the author as part of his research activities.

The author presented the paper "Ferrimagnetic composites in building material for electromagnetic wave absorption wireless communication systems" at the 4th IEEE European conference on antennas and propagation in Barcelona, Spain, 12-16 April 2010 [20].

The author Johann Christiaan Pretorius and co-author B.T. Maharaj published the ISI journal article: "Electrolytic manganese dioxide for EMW shielding effectiveness improvement of cement-based composites in indoor wireless communication systems" in the *International Journal of Physical Sciences*, vol. 8(8), pp. 295-301, February 2013 [21].

1.5 DISSERTATION OUTLINE

In Chapter 1 an introduction to the research is given with a motivation and research question. The objective of the research is discussed and an overview of the authorâĂŹs contributions and outputs are given.

In Chapter 2 a background and literature review is given. Published literature on SE is reviewed. The background of EMW absorber material is given and an overview of the published literature on various absorber materials is given. Shielding with building material and the absorption of EMW in buildings is discussed. An overview is given of the measurement methodologies used in literature. The background of EMW propagation and SE theory is discussed and the chapter ends with a conclusion.

In Chapter 3 the methodology of this research is given. The simulation of the propagation of EMW through composite material is discussed. The chapter explains the preparation of the samples used in the research. An overview of measuring techniques is given and the measurement methods and equipment used in this research are discussed. The chapter ends with a conclusion of the methodology used in this research.

Chapter 4 is a discussion of the measured results of this research. The measured SE of electrolyte manganese dioxide and MnZn ferrite composite cement-based material samples is given and discussed. The effect of the moisture content of the samples on the measured SE results is given and discussed. The measured results of the reflection loss and attenuation of the samples are discussed. The measured results are compared with the

simulated results and the findings discussed. A conclusion of the chapter is also given.

Chapter 5 is a conclusion of this research and recommendations for further study is given. The dissertation is ended by a detailed list of references.

CHAPTER 2

BACKGROUND AND LITERATURE REVIEW

2.1 LITERATURE REVIEW

A literature study is done to identify the latest research that has been conducted on a particular topic. This study covered several sections of EMW absorbtion:

- Shielding effectiveness
- Absorber material
- Measurement methodologies
- Shielding with building material
- Absorption in buildings

2.1.1 Shielding effectiveness

Electromagnetic interference (EMI) shielding refers to the reflection, absorption and attenuation of EMW radiation by material that acts as a shield against radiation. The primary mechanism of shielding is reflection. Accordingly, the shield has to be electrically conductive for reflection as a result of mobile carriers such as free electrons and holes

[22]. Absorption attenuation is the second mechanism of shielding. It is also known as the skin-effect attenuation within the thickness of the material. The shield should have electric and magnetic dipoles that interact with the electromagnetic fields in the material. The electric dipoles have a high value of dielectric constant, while the magnetic dipoles have high magnetic permeability. The absorption loss is an attenuation and is a function of the product $(\sigma_r \mu_r)$ while the reflection loss is a function of (σ_r/μ_r), with σ_r being the electric conductivity relative to copper and μ_r the relative magnetic permeability. A third mechanism contributing to SE is multiple internal reflections and attenuations [23]. Hence, SE can be calculated by obtaining the sum of the contributions of the three mechanisms.

The way in which the EMW shields transmit plane EMW is analogous to the transmission of electrical current and voltage by a two-wire transmission line [7]. The transmission equations for a transmission line with series impedance Z, and shunt admittance Y per unit length complex constants, are:

$$\frac{dV}{dx} = -ZI \tag{2.1}$$

$$\frac{dI}{dx} = -YV \tag{2.2}$$

The analogous equations for a plane EMW transmitted through a shield are:

$$\frac{d\boldsymbol{E}}{dx} = -j\omega\mu\boldsymbol{H} \tag{2.3}$$

$$\frac{d\boldsymbol{H}}{dx} = -(\sigma + j\omega\varepsilon)\boldsymbol{H} \tag{2.4}$$

where μ is the initial magnetic permeability, ε the dielectric permittivity, and σ the electrical conductivity.

2.1.2 Absorber material

2.1.2.1 Polymer material

It has been found that doping of a polymer with p-type or n-type impurities increases its conductivity by several orders of magnitude. High conductivity combined with the light-weight and high mechanical strength of the polymers make them attractive for high frequency shielding applications. The plain wave shielding behaviour of laminated shields constructed with these polymers and materials like copper and aluminium as a function of frequency was studied by [24]. Conductive polymer shielding is used in high data rate applications and aerospace where weight is a constraint. A 1 mm thick lamination of three layers, consisting of a combination of conductive polymer and conducting materials like copper and aluminum, was used. Computations for various combinations of copper-polymer-copper, polymer-copper-polymer, aluminium-polymer-aluminium, and polymer-aluminum-polymer were done. The polymer used was polyacetylene doped with 80% weight iodine.

2.1.2.2 Test system for polymer material

The reflection and transmission formulation by a planer multilayer was applied to compute the SE of the laminated conductive shields. Equation (2.82) was used to develop the SE theory for a multiple laminated sheet with three layers.

The transmission coefficient T for a three-layer laminated sheet is

$$T = \frac{2\eta_0 2\eta_1 2\eta_2 2\eta_3}{(\eta_0+\eta_1)(\eta_1+\eta_2)(\eta_2+\eta_3)(\eta_3+\eta_0)} \tag{2.5}$$

with η_1, η_2 and η_3 the intrinsic impedance of layers 1, 2 and 3 respectively.

The reflection coefficient Γ across the four mismatched interfaces of a three-layer laminated sheet is the product of the reflection coefficient at each interface:

$$\Gamma = (\frac{\eta_0 - \eta_1}{\eta_0 + \eta_1})(\frac{\eta_1 - \eta_2}{\eta_1 + \eta_2})(\frac{\eta_2 - \eta_3}{\eta_2 + \eta_3})(\frac{\eta_3 - \eta_0}{\eta_3 + \eta_0}) \tag{2.6}$$

2.1.2.3 Results for polymer material

The computed results of the SE as a function of frequency for the different combination of materials indicated that the material can perform well as a shield, although no experimental measurements were done to verify the calculations. Although the study did not specify the absorption loss, reflection loss and attenuation calculated to determine the SE, the calculated SE for the various models was higher than 200 dB at frequencies above 800 MHz. As the different components of the calculated SE were not specified, it is not possible to classify the used models as absorbing shields or reflecting shields.

It is shown by [25] that the absorption of a sheet does not depend on polarisation and that the shield is optimal when the angle of incidence and polarisation are arbitrary. The designed shield shows that half of the incident power is absorbed but no measurement data was available for verification.

2.1.2.4 Ferrite material

Hexagonal ferrites are known to exhibit the phenomenon of natural ferromagnetic resonance only at frequencies higher than approximately 2.5 GHz and up to 200 GHz, because their internal field of magnetic crystallographic anisotropy ranges from a few units to dozens of kilo-oersted [26], [27], and [28]. At lower frequencies, hexa ferrites do not substantially absorb EMW energy, and have high reflection. Spinal ferrites known to be soft ferrites with high permeability, absorb EMW energy at lower frequencies as a result of the high imaginary part of the complex permeability, which is a function of frequency. Neither hexagonal ferrites, nor spinal ferrites absorb EMW energy effectively in the frequency range

of 100 MHz to 2.5 GHz. However, absorption in this range can be achieved by increasing dielectric loss in the mixture of ferrites and the base material. The dielectric loss in NiZn and MnZn composite ferrites can be increased by the inclusion of conducting particles, such as carbon, in the mixture.

Material containing different types of ferrites or metal particles, fibres or manganite powders improves the control over the complex permittivity and permeability of the material. The reflection coefficient is a function of the ratio $\frac{\varepsilon_r}{\mu_r}$, and the transmission coefficient depends on the absolute value of μ_r [29]. It is shown that material with dominant magnetic losses is thinner and exhibits improved absorption behaviour. However the calculations have not been verified by experimental findings.

Carbon and MnZn ferrite was used to prepare a sheet-type EMW absorber, with chlorinated polyethylene being used as a binder. The absorber was fabricated by using an open roller [30], and was developed for an electric toll collection system at 5.8 GHz. Results of the 3.38 mm thick sample showed absorption of up to 20 dB at the operating frequency.

A two-layer EMW absorber, with short metal fibres in a ferrite-resin mixture and providing a bandwidth improvement in the GHz range, was developed by [31]. The metal fibres used were brass and measured 1 to 4 mm in length and 60 μm in diameter. The fibre lengths chosen were half the wavelength of the frequency of operation.

Wooden panels manufactured from thin laminated layers of wooden film impregnated with magnetic fluid were developed by [15]. The laminated wood was dried before it was placed under a pressure reduction of 5.3 kPa for $2\frac{1}{2}$ hours to create a vacuum in the conduit and trached pipes in the wood. The wood was then pressurised at 686.5 kPa for another $2\frac{1}{2}$ hours in the magnetic fluid.

Another type of wooden panel was manufactured by [32] and [9] by sandwiching magnetic powder between thin wooden layers. The SE and effective frequency of the panel can be controlled by changing its thickness and the composition of the magnetic powder.

The magnetic powder used is MnZn ferrite and stainless steel, and the resulting magnetic wood can be used to prevent radio interference in indoor wireless local area networks LANs which mainly use the 2.4 GHz frequency band.

A ferrite absorber for building walls in Japan was developed to suppress the reflection of VHF and UHF television signals in an effort to solve the problem of ghost images [19]. The absorber panel consists of ferrite fins and building material constructed so as to model a glass curtain wall.

2.1.2.5 Test system for ferrite material

In [26], washer-shaped samples were manufactured using ferrite, graphite and ferrite-graphite with paraffin as the base material. The ferrite used was of the MnZn ferrite type. The washer-shaped samples were approximately 14 mm in thickness and the absorption was found to be proportional to the total mass of ferrite. All samples were prepared with the same mass which resulted in slight variations in thickness. Subsequently, the samples were placed in a coaxial fixture with diameters of 16 and 7 mm. The transmission coefficient in the line was measured between 1 and 2.4 GHz and the absorbed power was calculated for each sample.

Cylindrical toroidal samples were also prepared by [28]. The samples, with 7 mm outer diameter, 3 mm inner diameter and 4 mm thickness, were prepared by mixing ferrite particles with an epoxy resin at an 85% weight content. The complex permeability and complex permittivity of the samples were measured by the transmission-reflection coaxial line method using an HP8722ES VNA system for frequencies from 2 GHz to 18 GHz.

2.1.2.6 Results for ferrite material

The results found by [26] for the washer samples show that the mechanism of absorption is a result of the ferrite particles. The graphite samples achieved an SE of 1 dB, the ferrite samples had an SE of 2.5 dB to 6.5 dB over the measured frequency range and the

ferrite-graphite samples 6 to 13.5 dB.

The results obtained by [28] are typical for ferrite, with the real and imaginary parts of its permeability retaining low values and the real part at 2.03.

Ferrite, graphite and carbon black were evaluated as EMW absorber materials in [33]. The measurements were done from 1.5 to 3 GHz. In the study, the materials were mixed with synthetic enamel and applied on a plate of expanded polystyrene (EPS). The characterisation was based on the determination of transmission and reflection characteristics. Two types of measurement technique were performed, the Naval Research Laboratory (NRL) arch technique and the insertion between antennae. The NRL arch technique was inconclusive owing to the peaks and valleys that were observed in adjacent frequencies. Two centre frequencies of 1.8 and 2.4 GHz each with a 300 MHz bandwidth were measured. Accordingly, it was found that graphite as an absorber material showed the best absorption of 5.7 dB at a frequency of 1.77 GHz.

2.1.2.7 Composite foils

Flexible foils with 0.5 to 1.5 mm thickness were developed in [34]. The foils consisted of polyethylene, carbon and inorganic fillers. Various fillers, such as ferrites, garnets, amorphous, nanocrystalline metals, dielectric, ferroelectric and piezoelectric ceramics, semiconductors, thermal and PTC resistor ceramics, and varistor ceramics, were also used. The broad spectrum of foils was developed for absorption, which was determined by their conductivity and permeability. It was found that the 1 mm thick foils absorb more than 30% of the incident power for frequencies above 40 MHz. Thus, foils can be prepared that hold optimal properties for given applications.

2.1.2.8 Test system for composite foils

Transmission and reflection measurements in [34] were done with a closed coaxial measuring technique in the 40 MHz to 1 GHz frequency range. The transmission loss from 700 MHz

to 18 GHz was measured using an open horn antenna setup. This setup cannot quantify the reflection loss owing to interference effects arising from the interaction between the antennae and its surroundings.

2.1.2.9 Results for composite foils

Transmission measurements were done from 700 MHz to 18 GHz and foils with 1 mm thickness absorbed more than 3 dB of the incident power [34]. The measured results showed that high SE of 21 to 34 dB can be achieved with 1 to 1.5 mm thick composite foils at 1 GHz, mainly as a result of high reflection losses. Samples with high absorption and lower reflection losses showed SE of 7 to 13.4 dB at 1 GHz.

2.1.2.10 Poly-vinylchloride composites with ferrite fillers

Poly-vinylchloride (PVC) polymer-based composites with different kinds of single ferrite fillers were examined by [35] and [36]. The complex permeability spectra and the EMW absorbing characteristics of MnZn/LiZn/PVC polymer composites were investigated by [35]. It was found that the complex permeablity had characteristic frequency dispertion which was attributed to two types of resonance mechanism: resonance of vibrating domain walls and natural ferromagnetic resonance of rotating magnetic moments in domains. It was also found that the triple ferrite MnZn/LiZn/PVC polymer composites are good EMW absorbers and are suitable for EMW suppression in mobile electronic equipment at frequencies above 100 MHz. Spinal ferrites, hexaferrites and metallic magnetic materials cannot be applied in the microwave region as absorbers because of the decrease in the magnetic loss (μ'') resulting from their Snoek limit. Ferrite polymer composite materials are suitable candidates for thin EMW absorbers in the *GHz* frequency range, because their Snoek limit is enhanced in the high frequency region.

The magnetic loss and permeability properties of different composites of MnZn ferrite ring samples were determined from direct current (DC) up to 10 MHz by [36].

2.1.2.11 Test system for PVC composite material

Polymer-based composites were produced by [35] by mixing the MnZn and LiZn ferrites in powder form with PVC powder. Toroidal 3 mm thick samples with a 9 mm outside diameter and a 3.6 mm inside diameter were then produced using a compression moulding process at 5 MPa and then thermally processing at 135°C for an hour. The complex permeability spectra were measured over the frequency range 10 kHz to 1 GHz using two VNAs at room temperature. The EMW-absorbing properties were then optimised by numerical simulations.

A wattmeter-hysteresis graph setup designed to cover many decades in the frequency range was used by [36]. An NF-HSA4101 power amplifier was driven with an Agilent 33220A function generator. The MnZn ferrite samples were prepared with outer diameters ranging from 15 to 5.9 mm and thicknesses ranging from 1.2 to 7 mm.

2.1.2.12 Results for PVC composite material

It was found by [35] that the value of μ'' is constant at low frequencies and, at frequencies above 1 MHz, drops rapidly to very low values. The reflection loss was calculated by [35] using the determined permeability values from 100 kHz to 1 GHz. In Table 2.1, the results of [35] show the frequencies at which the air-material interface was optimised by matching the impedances at the input interface for absorption.

Results obtained by [36] showed that the permeability of MnZn ferrite decreased to very low values at frequencies above 1 MHz. This finding is consistent with the findings of other research done.

2.1.2.13 Conductive and carbon composite material

The EMW dissipation capabilities of cement mortar were improved by replacing small amounts of the fine aggregate with bamboo-charcoal as a conductive filler by [12]. The SE of the cement mortar was improved from 2 dB, with no carbon filler up to 20 dB, with the

Sample	Matching frequency (MHz)
1.0 MnZn	344
0.8 MnZn + 0.2 LiZn	522
0.5 MnZn + 0.5 LiZn	714
0.2 MnZn + 0.8 LiZn	845
0.1 LiZn	938

Table 2.1: EMW absorption properties of MnZn/LiZn/PVC samples

carbon filler in the frequency range 100 MHz to 400 MHz.

Multiwalled carbon nanotubed (MWCNT) filled polyacrylate composite was coated 1.5 mm thick on 60×60×5 cm concrete panels and tested for EMI shielding applications by [37]. MWCNT has excellent electrical and mechanical properties. Pure acrylic emulation is weather resistant and a universal choice for making alkali-resistant paints for internal applications. The polyacrylate is non-conductive on its own.

Concrete walls reinforced with metallic grids have been investigated for many years [17]. Conductive concrete, which consisting of a cementious composite with a low volume concentration of steel fibres included in the cement mixture, was investigated by [18].

2.1.2.14 SE by cavity and interface mismatch

By creating small cavities in the cement mortar by adding small 1 mm expanded polystyrene (EPS) spheres to the mixture, [6] increased the SE by increasing the multiple reflections and attenuations inside the material. Accordingly, the EPS beads scatter the incident wave and reflection losses of up to 10 dB in the 8 GHz to 18 GHz frequency range were measured. A volume increase (up to 60%) in the EPS in the cement mixture was accompanied by an increase in reflection loss.

A three-layer EMW absorber was designed using building material only by [16]. The

third layer was an air gap placed between the two outer layers of fibre reinforced building material.

Two low-loss parallel slabs consisting of stratified construction materials with different dielectric constants were used to construct an absorbing shield by [38]. The wave shielding happens at the interface of the two materials. The two materials used were acrylic resin and glass and the SE was controlled by the thickness ratio of the two materials and had a narrow bandwidth.

A 2 to 5 cm sandwich-like panel, with a substrate consisting of polyurethane phenolic material with both sides covered with smooth aluminium foil or polyester for shielding in buildings against mobile communication systems, was developed by [39].

2.1.3 Measurement methodologies in the literature

Reflection measurement based on a monostatic configuration was performed in an anechonic chamber of 4 m in length by [40]. The setup consisted of four similar horn antennae which were positioned 3 m in front of the test sample. The sample was placed on a polystyrene-covered pylon situated 1 m from the back of the chamber. This antenna array allowed for different polarisation measurements. These measurements were done in the 8 to 12.5 GHz range. Various homogeneous single-layer samples were studied, measuring 170×170 mm. To determine the complex permittivity, three measurements were done with the same antenna setup. Firstly, the S_{11} parameter was measured using a flat metallic plate that was the same size as the samples. This measurement was used as the reference. Secondly, S_{11} was then measured with the sample in front of and against the metalic plate. Thrirdly, S_{11} was measured with the sample in place but without the metallic plate. An optmisation algorithm was developed using a gradient algorithm and the data obtained from the three measurements and the theoretical data.

The reflective properties of materials were characterised in specular direction by [2]. The transmitting antenna (Tx) and receiving antenna (Rx) in Figure 2.1 are moved along a

circle with a radius of 0.7 m placing the sample in the centre of the circle. The measured angles were limited to between 20° and 60° owing to the cable lengths. The incidence angle φ_i and the reflective angle φ_r were kept equal.

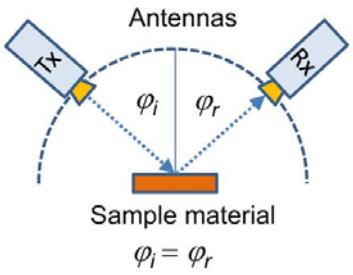

Figure 2.1: Setup to measure reflective properties of materials by [2]

A time domain simulation of magnetic media was developed by [41]. This simulation was based on incorporating a non-linear system into the transmission line modeling (TLM) method. Subsequently, the frequency dependent permeability was described using a multiple Debye approximation and the saturation of the magnetisation was modelled using the Ising spin formulation of equation (2.46).

A windowed semi-anechoic box method is used by [42] to remedy the deficiencies of time-domain test methods of SE. The results found showed that the method can be used to distinguish the SE performance of different materials for each frequency component and to evaluate the overall shielding performance of materials against electromagnetic pulses.

Transmission and reflection frequency domain measurements were done to determine the electromagnetic properties of solid material by [43] and [44]. Accordingly, the complex relative permittivity ε_r and complex relative permeability μ_r were determined simultaneously. This method is known as the Nicolson-Ross-Weir (NRW) method, and uses the S parameters to obtain ε_r and μ_r from equations (2.55) to (2.63).

An efficient three-dimensional geometry and image technique multi-array propagation model was used to trace multiple signal rays from the transmitter to the receiver by [45]. This method solved the problem of requiring numerous ray-object intersection tests and

extensive data arrays for ray tracing which demands lengthy computation time and many resources to obtain satisfactory results. However, the model becomes cumbersome for complex geometry and for large numbers of reflections.

The traditional definition and measurement methods for SE are adequate when the radiation is from a narrowband EMW source. However, they are not necessarily valid for wideband (WB) and ultra wideband (UWB) sources, because it is not always valid to associate the effectiveness of the source with the peak or average power of the target as defined by a local point in space. A new method was presented for characterising the SE of a building and found to be more encompassing than a limited point measurement by [46]. Three different CW source locations were used with multiple source elevations. Simulations were run prior to taking measurements to determine the number of test points required to capture the electric field distribution in a building.

A SPICE program transmission line model was employed in simulations on materials with known properties. This model was based on Schelkunoff isomorphism, assuming that attenuation in shielding material depends on material conductivity and magnetic permeability by [47]. The inductance (L) and capacitance (C) transmission line parameters in Figure 2.2 were determined assuming that C corresponds with the permittivity ε and L with the permeability μ. The resistive element (R) was determined by the natural analogy between electricity travelling through a conductor and an EMW propagating through a conductive medium. The data obtained from the SPICE simulation was verified by using a waveguide-based measurement setup to test a wide selection of materials with known electromagnetic characteristics. The samples were also tested with an antenna system. Good correlation was found between the SPICE model, and the waveguide-based and antenna-based systems.

2.1.4 Shielding with building material

Shielding of an EMW can be defined as the reflection and/or absorption and attenuation of EMW radiation by a material that acts as a shield [22]. Three different types of typical

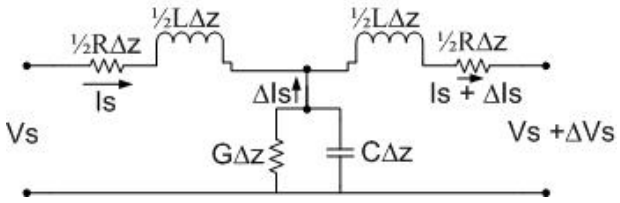

Figure 2.2: RLCG transmission line model

building material were modelled in a field calculation tool based on the method-of-moments technique by [48]. The material comprised low reflective plasterboard, high reflective plasterboard, and ferroconcrete. The low reflective plasterboard contained a steel frame, plaster cement, heat insulation, and a moisture barrier of polyethylene foil. In the high reflective plasterboard the polyethelyne foil was replaced by aluminium foil which resulted in high reflectivity. The concrete body of the ferroconcrete was reinforced by a steel bar mesh. The moisture in the concrete increased the reflectivity of the sample. The calculations and measurements were done from 50 MHz to 1 GHz and showed that the SE is mainly as aresult of reflection. In the low reflective sample, the SE is less than 10 dB in the 800 MHz to 1 GHz range, and between 10 and 40 dB for the high reflective samples.

Ferroconcrete is reinforced with steel mesh and standard concrete. The attenuation factor and corner frequency depend directly on the electrical parameters of the system. A shield behaves similarly to an electrical transfer system [49]. Subsequently, the system parameters were applied in an analytical model.

The absorption capability of cementatious composites was increased by [50] by reducing the reflection loss by impedance matching with a silica fume mortar layer. This double-layer absorber has an MnZn ferrite mortar layer as a second layer for attenuation. Measurements between 2 and 18 GHz showed reflectivity of less than -10 dB. However, the authors made no mention of absorption, attenuation or SE in their results.

Cement mortar was upgraded with conductive matter by [12] to improve the absorption or dissipation capabilities for EMW. It was found that the replacement of a small

amount of the fine aggregate in cement mortar with bamboo-charcoal did not affect the mechanical strength of the material. A series of test experiments for the SE of the cement mortar panels with various parameters was carried out, and he thickness and replacement ratio of the bamboo-charcoal were varied. The measurements were done from 30 MHz to 1.5 GHz, and it was found that with 7% replaced aggregate, the SE value can have peaks as high as 18 dB. The influence of the variation in thickness was not obvious in the study. The bamboo-charcoal has electrical conductivity, which makes this method of shielding mainly because of reflection and the EMW absorption and attenuation by the material was not reported in the study.

The EMW-absorbing effectiveness of carbon black (CB) cement-based composites (CBCC) was studied by[14]. Measurements were done from 8 to 26 GHz, and the comprehensive strength, electrical properties and absorbing coefficient of the CBCC, containing different contents of CB, were studied. The conductive network within the CBCC can be formed by using a small amount of CB. It was founf that the comprehensive strength of the CBCC decreases with an increase of CB content. The CBCC with 2.5 wt.% CB has a -10 dB reflectivity bandwidth of 15 to 26.5 GHz. The CB improved the loss factor of the CBCC which resulted in polarisation absorption.

The SE of a densified small particle (DSP) cement composite was investigated by [51] using the nested reverberation chamber (NRC) method. Accordingly, different loading ratios were measured. The success of the DSP cementatious composite was based on the use of water-soluble polymers and ultra fine solid particles consisting of amorphous silica. The SE was improved by adding graphite powder and stainless steel fibres separately. The samples were manufactured by mixing the DSP cement composite with various ratios of the graphite and stainless steel fibres and, the SE of the samples was measured by the increasing evaporation of fluid components. Empirical asymptotic limits of SE were found for the material used in the samples, which is important for the long-term shielding performance of architectural structures.

Continuous basalt fibres, spherical expansion perlite with closed pores and graphite,

were used as components and combined with space wave impedance matching to improve the absorption of new cement-based microwave absorbing materials [52]. Thus a minimum reflectivity of -10 dB over a 4 GHz bandwidth was achieved. Cement-based materials are typical structural materials. The matching problem between wave absorbing components and cement results in the instability of the interface between cement and hydration products. This instability leads to the decline of mechanical properties. The measurements were done from 8 to 18 GHz with a minimum of -10 dB reflectivity from 14 to 18 GHz.

Magnetic wood laminated with ferrite powder and stainless steel powder can be used as a building material and is a suitable quality for indoor EMW absorber application [9], [32] and [15]. It was found that the centre frequency of the shield shifted to the lower frequencies when the thickness of the shield is increased. The half bandwidth also increased with the increased thickness of the magnetic layer. The magnetic layer thickness, the ratio of ferrite powder to stainless steel powder and the volume content of magnetic powder significantly influence the frequency band width and the EMW absorption. The laminated magnetic wood is manufactured by using vinyl plastic acetate emulsion adhesive as an intermediate agent to mix MnZn-ferrite powder and stainless steel powder, which is then sandwiched between two pieces of fibre board.

The Friis formula indicates that propagation losses increase with an increase in frequency but it was found that the losses are the same at both 2.4 and 5 GHz, the two WLAN frequencies. Various standard building materials were evaluated in an anechoic chamber [53], and the scattering parameters of each material sample in the propagation path were measured. Measurements were done from 2 to 7 GHz.

A dispersion model that accounts for the complex permittivity dependency on frequency was implemented for concrete [54]. The concrete was modelled as a Debye material with a dc electrical conductivity and dielectric material with constant effective permittivity in a numerical simulator based on the transmission line modelling method and the finite integration technique. The magnetic permeability was deemed equal to that of free space because concrete is a nonmagnetic material. Subsequently, the numerical simulations

were compared with an analytical approach to the SE of concrete structures based on the Schelkunoff theory with approximated expressions for reflection, absorption and multiple reflection losses. It was found that the analytical approach is far more computationally efficient than the numerical model and that it provided an insight into the SE mechanism.

Various concentrations of MnO_2 were used as magnetic material filler in cement-based pallets to increase the SE of building material. The sintered pallets was characterised for its dielectric and SE properties by [55]. A high dielectric constant of 300 at 1 MHz and 25 at 200 MHz and a SE of 2 to 9 dB for frequencies between 8 and 13 GHz was measured. The test setup used a transmit setup with a signal generator and antenna. The receiving setup used consisted of a spectrum analyser and antenna. The test sample was placed in between the two antennae.

2.1.5 Absorption in buildings

Electromagnetic pollution has been categorised as a new form of pollution [56], because it is as detrimental to society as air and water pollution. EMW radiation has increased millions of times in the last few decades, and the scientific community is devoting increasing attention to this environmental problem. Radiation from GSM and other radio sources produces interference that can cause sensitive equipment to malfunction. The SE of buildings has been investigated by many researchers. Furthermore, various approaches have been followed to measure SE and the advantages and disadvantages of the different methods identified.

One method for evaluating the EMW SE of a commercial building is presented by [57]. These authors addressed the issues of extensive and costly tests, access to transmission points and the constraints of commercial building illumination. This was done by using the existing EM signals present in buildings such as AM and FM radio signals and cellular phone tower transmissions. Measurements were taken outside the building in order to characterise the environment, to identify strong signals from each frequency band and to constitute the incident EMW signals. The identified frequencies were then measured inside the building at various positions. The researchers then determined the SE by using the

incident and internal measured signal strengths. The results are not discussed however and the validation of this method cannot be verified.

The ability of an enclosure or building to reduce emissions of EMW by means of its SE is compromised by the walls of the enclosure, the slots and apertures for heat dissipation, cable penetration, and peripherals. One method to optimise the EMW shielding of a room was developed by [58]. This was done using minimum absorbing materials in suitable predetermined positions on the inner surfaces of the walls. A room with 20% covered walls showed 17 dB SE for frequencies up to 1 GHz. In this case the absorber material was solid ferrite tiles 6 mm thick.

In [46], a shielding difference calculation was used instead of the traditional point-to-point SE calculation. Empirical test data taken with a continuous wave (CW) source on a reconfigurable building was presented and compared with simulated data, which was generated using the method-of-moments code. The average electric field of multiple locations of measurement was computed for each discrete frequency in the CW sweep in the building. The difference between the average electric field with shielding and without shielding constitutes the shielding difference. However, this paper only refers to measurements up to 200 MHz. Although the results are not relevant to this research study, the research shows that the method is viable for determining the SE of a building.

The experimental SE of shielding rooms with various layered walls, which were built using different conductive cement-based materials, were measured by [59] and [60]. The research does not, however, mention the material type used to increase the conductivity of the cement-based 30 cm thick walls. The research did show that SE increases with an increase in conductivity.

To shield a particular frequency range of radio signals, such as wireless LAN, frequency selective surfaces (FSS) can be applied to the walls, ceiling and floor of an indoor zone. The extent of radio isolation provided by a shielded dividing wall between two rooms was evaluated by [61]. Accordingly, radio isolation of 12 and 10 dB was measured at 5.8

and 2.45 GHz respectively. Diffracted energy leaking through the windows was still found to be present.

The aperture shapes of doors, windows, air-conditioning ducts and cable holes are sources of EMW penetration into buildings. Thirteen different aperture shapes for doors were tested to select the best shape for maximum SE for cellular communication frequencies by [11]. It was found that covering the doorway with a curved wall increases the SE, because the path length through the curved wall is longer than through the straight wall.

2.2 ELECTROMAGNETIC WAVE PROPAGATION

The history of magnetism began with the discovery of the properties of a mineral called magnetite (Fe_3O_4). The most plentiful deposits of this material were found in the district of Magnesia in Asia Minor before the birth of Christ. At that time it was observed that these naturally occurring stones would attracted iron [62]. Later on magnetite was used in the lodestone of early navigators. In 1600, William Gilbert published *De Magnete*, the first scientific study on magnetism. In 1819, Hans Christian Oersted observed that an electric current in a wire affected a magnetic compass needle; thus, with later contributions by Faraday, Maxwell, Hertz and others, the new science of electromagnetism came into being.

Through experimental research Michael Faraday found that a changing magnetic field produces an electric field. James Clerk Maxwell was inspired by Faraday's experimental work and, while working alone at his home in Scotland, found that a changing electric field produces a magnetic field. The interdependence of electric fields and magnetic fields is what produces an EMW. It is this interdependence of electric fields and magnetic fields in an EMW that will be exploited during this research project which intends to cancel or attenuate an EMW.

The transmission of any sort of information by electrical means involves the propagation of energy by an EMW. EMW propagation depends on the way in which the vector quantities, electric field and magnetic field vary in space and time. The vector equations

relating to these quantities are Maxwell's equations. This section will discuss the existence and characteristics of EMWs in free space.

The electric and magnetic fields in a time-varying situation are related to each other by Maxwell's equations and can be written as:

$$\nabla \times \boldsymbol{E} = \frac{-\partial \boldsymbol{B}}{\partial t} \tag{2.7}$$

$$\nabla \times \boldsymbol{H} = \frac{-\partial \boldsymbol{D}}{\partial t} + \boldsymbol{J} \tag{2.8}$$

$$\nabla \bullet \boldsymbol{B} = 0 \tag{2.9}$$

$$\nabla \bullet \boldsymbol{D} = \rho \tag{2.10}$$

In these equations, $\boldsymbol{D}$ is the electric displacement, $\boldsymbol{E}$ is the electric field strength, $\boldsymbol{B}$ is the magnetic flux density and $\boldsymbol{H}$ is the magnetic field strength. These are all functions of position and time. The remaining symbols are ρ, the electric charge density, and $\boldsymbol{J}$, the electrical current density. These four equations form the basis of electromagnetic theory.

The auxiliary equations relate $\boldsymbol{D}$ to $\boldsymbol{E}$ and $\boldsymbol{B}$ to $\boldsymbol{H}$ and are given by:

$$\boldsymbol{D} = \varepsilon \boldsymbol{E} \tag{2.11}$$

$$\boldsymbol{B} = \mu \boldsymbol{H} \tag{2.12}$$

With ε the dielectric constant or permitivity and μ the magnetic permeability, the conduction current density is:

$$\boldsymbol{J} = \sigma \boldsymbol{E} \tag{2.13}$$

In addition the convection current density is:

$$\boldsymbol{J} = \rho \upsilon \tag{2.14}$$

With σ the conductivity, ρ the volume charge density and υ the velocity.

In order to consider wave motion in free space, Maxwell's equations may be written in terms of $\boldsymbol{E}$ and $\boldsymbol{H}$ using equations (2.11) to (2.14).

$$\nabla \times \boldsymbol{H} = \varepsilon_0 \frac{-\partial \boldsymbol{E}}{\partial t} \tag{2.15}$$

In equation (2.15), ε_0 is the permittivity in free space. Equation (2.15) states that if $\boldsymbol{E}$ is changing with time at some point, then $\boldsymbol{H}$ has curl at that point and thus can be considered as forming a small closed loop linking the changing $\boldsymbol{E}$ field. Also if $\boldsymbol{E}$ is changing with time, then $\boldsymbol{H}$ will in general also change with time, although not necessarily in the same way.

$$\nabla \times \boldsymbol{E} = -\mu_0 \frac{-\partial \boldsymbol{H}}{\partial t} \tag{2.16}$$

In equation (2.16), μ_0 is the permeability in free space. Equation (2.16) states that the changing $\boldsymbol{H}$ produces an electric field, which forms small closed loops about the $\boldsymbol{H}$ lines. This results once more in a changing electric field, but this field is presented at a small

distance away from the point of the original disturbance. The velocity with which the effect moves away from the original point is the velocity of light.

The divergence of $\boldsymbol{E}$ and the divergence of $\boldsymbol{H}$ can be written as:

$$\nabla \bullet \boldsymbol{E} = 0 \tag{2.17}$$

$$\nabla \bullet \boldsymbol{H} = 0 \tag{2.18}$$

Maxwell's equations for sinusoidal variation with time in free space can be accomplished by complex notation and phasors, and can be written as:

$$\nabla \times \boldsymbol{H}_s = j\omega\varepsilon_0 \boldsymbol{E}_s \tag{2.19}$$

$$\nabla \times \boldsymbol{E}_s = -j\omega\mu_0 \boldsymbol{H}_s \tag{2.20}$$

$$\nabla \bullet \boldsymbol{E}_s = 0 \tag{2.21}$$

$$\nabla \bullet \boldsymbol{H}_s = 0 \tag{2.22}$$

The symbol s indicates a frequency domain quantity expressed as a function of the complex frequency s. Only cases where s is purely imaginary, $s = j\omega$, are considered.

Making use of Euler's identity $e^{j\omega t} = cos\omega t + jsin\omega t$, the x (vertical) component of $\boldsymbol{E}_s$ propagates in the z direction and becomes:

$$E_x = E_{x0} cos[\omega(t - z\sqrt{\mu_0 \varepsilon_0})] \tag{2.23}$$

Equation (2.23) E_{x0} is the value of E_x at $z = 0$ and $t = 0$. The radical $\sqrt{\mu_0 \varepsilon_0}$ is the reciprocal of c, the velocity of light in free space. H_y is perpendicular (horizontal) to and accompanies E_x; it travels in the z direction and can be written as:

$$H_y = E_{x0} \sqrt{\frac{\varepsilon_0}{\mu_0}} cos[\omega(t - z\sqrt{\mu_0 \varepsilon_0})] \tag{2.24}$$

The ratio of the electric to magnetic field intensities given by (2.23) to (2.24) is the intrinsic impedance of free space and can be written as:

$$\frac{E_x}{H_y} = \eta_0 = \sqrt{\frac{\varepsilon_0}{\mu_0}} = 120\pi\Omega \tag{2.25}$$

This uniform plane wave is a transverse electromagnetic (TEM) wave that represents an energy flow in the positive z direction. If the TEM wave propagates in a material with magnetic properties (μ), dielectric properties (ε) and conductivity, then Maxwell's curl equations become:

$$\nabla \times \boldsymbol{H}_s = (\sigma + j\omega\varepsilon)\boldsymbol{E}_s \tag{2.26}$$

and

$$\nabla \times \boldsymbol{E}_s = -j\omega\mu \boldsymbol{H}_s \tag{2.27}$$

The electric and magnetic field intensities propagating in the +z direction can be written in complex exponential notation:

$$E_{xs} = E_{x0}e^{-\gamma z} = E_{x0}e^{-\alpha z}e^{-j\beta z} \tag{2.28}$$

and

$$H_{ys} = \frac{E_{x0}}{\eta}e^{-\gamma z} = \frac{E_{x0}}{\eta}e^{-\alpha z}e^{-j\beta z} \tag{2.29}$$

In equations (2.28) and (2.29) $\gamma = \alpha + j\beta$ the complex propagation constant, α the attenuation constant, β the phase constant, and η the intrinsict impedance of the material. The propagation constant can be written as:

$$\gamma = \alpha + j\beta = j\omega\sqrt{\mu\varepsilon}\sqrt{1 - j\frac{\sigma}{\omega\varepsilon}} \tag{2.30}$$

The intrinsic impedance in the material is complex and can be written as:

$$\eta = \sqrt{\frac{j\omega\mu}{\sigma + j\omega\varepsilon}} = \sqrt{\frac{\mu}{\varepsilon}}\frac{1}{\sqrt{1 - j(\frac{\sigma}{\omega\varepsilon})}} \tag{2.31}$$

2.2.1 Reflection coefficient and transmission coefficient

For applications of practical interest, material regions of finite size will be investigated. The phenomenon of reflection occurs when a uniform plane wave is incident on the boundary between regions composed of two different materials with different permeability, permittivity and conductivity as shown in Figure 2.3. From (2.28), the incident wave travelling in the

$+z$ direction in region 1 toward the boundary surface at $z = 0$ can be given by:

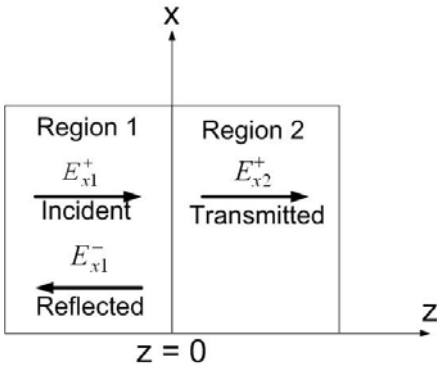

Figure 2.3: Boundary between two regions composed of different materials

$$E^+_{xs1} = E^+_{x10} e^{-\gamma_1 z} = E^+_{x10} e^{-\alpha_1 z} e^{-j\beta_1 z} \tag{2.32}$$

The magnetic field that is associated with E^+_1 is from (2.29):

$$H^+_{ys1} = \frac{E^+_{x10}}{\eta_1} e^{-\gamma_1 z} = \frac{E^+_{x10}}{\eta_1} e^{-\alpha_1 z} e^{-j\beta_1 z} \tag{2.33}$$

With the propagation direction of the incident wave perpendicular to the boundary plane, it can be referred to as normal incidence. Energy will be transmitted across the boundary surface at $z = 0$ into region 2, and the wave propagating in the $+z$ direction in region 2 is:

$$E^+_{xs2} = E^+_{x20} e^{-\gamma_2 z} = E^+_{x20} e^{-\alpha_2 z} e^{-j\beta_2 z} \tag{2.34}$$

$$H^+_{ys2} = \frac{E^+_{x20}}{\eta_2} e^{-\gamma_2 z} = \frac{E^+_{x20}}{\eta_2} e^{-\alpha_2 z} e^{-j\beta_2 z} \tag{2.35}$$

This wave propagates away from the boundary surface into region 2 and is the transmitted

wave. To satisfy the boundary condition at $z = 0$, the total electric field intensity has to be continuous $(E_{xs1} = E_{xs2})$, which requires a wave travelling away from the boundary in region 1. This wave is the reflected wave and travels in the $-z$ direction:

$$E_{xs1}^{-} = E_{x10}^{-} e^{\gamma_1 z} = E_{x10}^{-} e^{\alpha_1 z} e^{+j\beta_1 z} \tag{2.36}$$

Therefore at $z = 0$:

$$E_{xs1}^{+} + E_{xs1}^{-} = E_{xs2}^{+} \tag{2.37}$$

and

$$E_{x10}^{+} + E_{x10}^{-} = E_{x20}^{+} \tag{2.38}$$

The accompanying reflected magnetic field intensity is:

$$H_{ys1}^{-} = -\frac{E_{x10}^{-}}{\eta_1} e^{\gamma_1 z} = -\frac{E_{x10}^{-}}{\eta_1} e^{\alpha_1 z} e^{+j\beta_1 z} \tag{2.39}$$

and

$$H_{ys1}^{+} + H_{ys1}^{-} = H_{ys2}^{+} \tag{2.40}$$

and therefore

$$\frac{E_{x10}^{+}}{\eta_1} - \frac{E_{x10}^{-}}{\eta_1} = \frac{E_{x20}^{+}}{\eta_2} \tag{2.41}$$

Solving (2.41) for E_{x20}^{+} and substituting into (2.38), the ratio of the amplitudes of the reflected and incident electric fields is the reflection coefficient:

$$\Gamma = \frac{E_{x10}^{-}}{E_{x10}^{+}} = \frac{\eta_2 - \eta_1}{\eta_2 + \eta_1} \tag{2.42}$$

The ratio of the amplitudes of the transmitted and incident electric fields is the transmission coefficient:

$$T = \frac{E_{x20}^{+}}{E_{x10}^{+}} = \frac{2\eta_2}{\eta_2 + \eta_1} \tag{2.43}$$

For a material in region 1 with thickness d, the total fields are:

$$E_{xs1} = E_{x10}^{+}(e^{-\gamma_1 d} + \Gamma e^{\gamma_1 d}) \tag{2.44}$$

and

$$H_{ys1} = \frac{E_{x10}^{+}}{\eta_1}(e^{-\gamma_1 d} - \Gamma e^{\gamma_1 d}) \tag{2.45}$$

The ratio of the total fields (2.44) and (2.45) is the input intrinsic impedance for region 1 [7]:

$$\eta_{in} = \frac{E_{xs1}}{H_{ys1}} = \eta_1 \frac{\eta_2\left(e^{\gamma_1 d} + e^{-\gamma_1 d}\right) - \eta_1\left(e^{\gamma_1 d} - e^{-\gamma_1 d}\right)}{\eta_1\left(e^{\gamma_1 d} + e^{-\gamma_1 d}\right) - \eta_2\left(e^{\gamma_1 d} - e^{-\gamma_1 d}\right)} = \eta_1 \frac{\eta_2 cosh\gamma_1 d + \eta_1 sinh\gamma_1 d}{\eta_1 cosh\gamma_1 d + \eta_2 sinh\gamma_1 d} \tag{2.46}$$

2.2.2 Electric and magnetic properties of material

There are two types of magnetic material: soft and hard [63]. Soft magnetic materials can be magnetised and demagnetised so that they can transfer or store magnetic energy. Hard magnetic materials are difficult to magnetise and demagnetise and are used as permanent magnets. The way magnetic material conducts magnetic flux in magnetic circuits is similar to the way conductors conduct electric current in electric circuits. The relative permeability μ_r is a measure of how much better a given material conducts magnetic flux than air. Most materials are poor conductors of magnetic flux. Magnetic materials undergo magnetisation when they are subjected to an applied magnetic field. This magnetisation depends on the structure of the atom involved.

The model of an atom can be used to explain the different behaviour of various types of material in magnetic fields. This atomic model, which assumes a central positive nucleus, is surrounded by electrons in various circular orbits. An electron in an orbit is analogous to a small current loop, because it is a moving charge and experiences a torque in an external magnetic field. The pattern of the magnetic field generated by a current loop is similar to a permanent magnet and can be regarded as a magnetic dipole with north and south poles. The magnetic field produced by an orbiting electron is aligned with the external magnetic field by the torque. All the orbiting electrons in the material will add their magnetic fields to the applied magnetic field and the resultant magnetic field at any point in the material will be greater than it would have been at that point if the applied magnetic field were not there. The orbiting electron generates an orbital magnetic moment m_o. Magnetic dipoles cause magnetisation.

Electron spin causes a second magnetic moment m_s of $\pm 9 \times 10^{-24} Am^2$, with the plus and minus signs indicating aiding or opposing alignment with an external magnetic field. Only the spins of electrons in unfilled shells will contribute to the magnetic moment of an atom.

Another contribution to the magnetic moment of an atom is made by nuclear spin.

This contribution is, however, of negligible effect. The different moments of the atoms determine the magnetic characteristics of a material. Therefore, the magnetic properties of a material are determined by the interaction of the magnetic dipoles of its atoms with an external magnetic field, and depend on its crystalline structure. In atoms with an even number of electrons, pairs of electrons have opposite spins, and the spin magnetic moments cancel out. By contrast, atoms containing an odd numbers of electrons have one unpaired electron and produce a spin magnetic moment. There are various types of magnetic material and they can be classified as follows: diamagnetic, paramagnetic, ferromagnetic, anti-ferromagnetic, ferrimagnetic, and super-paramagnetic.

2.2.2.1 Diamagnetic material

Diamagnetic material has atoms in which the small magnetic fields produced by the motion of the electrons in their orbits and the magnetic fields produced by electron spin, combine to produce a net field of zero in the absence of an external magnetic field.

This material may also be described as one in which the permanent magnetic moment of each atom is zero. An external magnetic field will produce no torque on the atom, no realignment of dipole fields and, consequently, an internal magnetic field that is about the same as the applied field. The applied magnetic field causes the spin moment to slightly exceed the orbital moment $(m_s > m_o)$, resulting in a small net magnetic field, which opposes the applied magnetic field.

Metallic bismuth shows a greater diamagnetic effect than most other diamagnetic materials, among which are hydrogen, helium, and the other inert gases, sodium chloride, copper, gold, silicon, germanium, graphite, diamond, lead, mercury, silver, and sulphur. The relative permeability (μ_r) of diamagnetic material is constant and independent of the applied magnetic field. Diamagnetic material has small and negative magnetic susceptibility resulting in $\mu_r < 1$.

A diamagnetic effect is present in all materials, because it arises from an interaction

of the external magnetic field with every orbiting electron; however, other effects in the materials considered next overshadow it.

2.2.2.2 Paramagnetic material

In paramagnetic material the effects of the electron spin and orbital motion do not quite cancel out. The magnetic susceptibility in such materialis primarily due to spin magnetic moments (m_s), and the atom as a whole has a small magnetic moment; however, the random orientation of the atoms in a larger sample produces an average magnetic moment of zero.

This material shows no magnetic effects in the absence of an external field. When an external magnetic field is applied, however, the magnetic moments are aligned in the direction of the applied field and there is a small torque on each atomic moment. These moments tend to become aligned with the external field. This alignment acts to increase the value of the applied field within the material over the external value.

However, the diamagnetic effect is still operating on the orbiting electrons and may counteract the above increase. If the net result is a decrease in the applied field, the material is still called diamagnetic, however, if there is an increase in the applied field, the material is termed paramagnetic. Paramagnetic elements include aluminium, calcium, chromium, magnesium, niobium, platinum, titanium and tungsten. Paramagnetic materials have a small and positive magnetic susceptibility, resulting in $\mu_r > 1$, and are independent of the applied magnetic field.

The rest of the materials to be discussed all have strong magnetic moments.

2.2.2.3 Ferromagnetic material

The interaction of adjacent atoms causes an alignment of the magnetic moments of atoms in either an aiding or exactly opposing manner. In ferromagnetic materials each atom has a relatively large dipole moment, caused primarily by uncompensated electron spin moments

(m_s) because the orbital magnetic moments (m_o) are almost zero.

Inter-atomic forces cause these moments to line up in a parallel fashion over regions containing large numbers of atoms. These regions are called domains, and they may have a variety of shapes and sizes, ranging from one micrometre to several centimetres, depend on the size and shape of the material, and the magnetic history of the sample. Ferromagnetic materials have a large positive magnetic susceptibility, resulting in $\mu_r >> 1$.

The overall effect of the adjacent atoms is one of cancellation, and the material as a whole has no magnetic moment. On application of an external magnetic field, however, those domains that have moments in the direction of the applied field, increase their size at the expense of their neighbours, and the internal magnetic field increases greatly in comparison with that of the external field as can be seen in Figure 2.4

When the external field is removed, a completely random domain alignment is not usually attained, and a residual, or remnant, dipole field remains in the macroscopic structure. The fact that the magnetic moment of the material is different after the applied field has been removed, or that the magnetic state of the material is a function of its magnetic history, is called hysteresis. The relative permeability of ferromagnetic materials is a function of both the applied field and the previous magnetic history.

The only elements that are ferromagnetic at room temperature are iron, nickel and cobalt, and they lose all their ferromagnetic characteristics above a temperature called the Curie temperature, which is $1043K$ for iron. Some alloys of these metals with each other and with other metals are also ferromagnetic such as, for example, alnico, an aluminum-nickel-cobalt alloy with a small amount of copper.

At lower temperatures some of the rare earth elements, such as gadolinium and dysprosium, are ferromagnetic. It is also interesting to note that some alloys of non-ferromagnetic metals are ferromagnetic, such as bismuth-manganese and copper-manganese-tin.

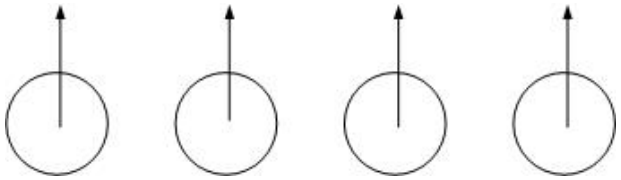

Figure 2.4: Structure of spin magnetic moment under an applied magnetic field in ferromagnetic material

2.2.2.4 Anti-ferromagnetic material

The forces between adjacent atoms in anti-ferromagnetic materials cause the atomic moments to line up in an anti-parallel fashion as shown in Figure 2.5. The net magnetic moment is zero, and anti-ferromagnetic materials are affected only slightly by the presence of an external magnetic field.

This effect was first discovered in manganese oxide, but several hundred anti-ferromagnetic materials have been identified since then. Many oxides, sulphides and chlorides are included, such as nickel oxide (NiO), ferrous sulphide (FeS), and cobalt chloride $(CoCl_2)$. Anti-ferromagnetism is only present at relatively low temperatures, often well below room temperature. However, the effect is not of engineering importance at present.

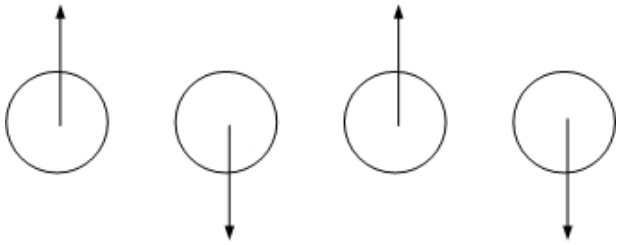

Figure 2.5: Structure of spin magnetic moment under an applied magnetic field in anti-ferromagnetic material

2.2.2.5 Ferrimagnetic material

Ferrimagnetic material also shows an anti-parallel alignment of adjacent atomic moments, but the moments are not equal as shown in Figure 2.6. A large response to an external

magnetic field therefore occurs, although not as large as that in ferromagnetic materials.

The most important group of ferrimagnetic materials are the ferrites, in which conductivity is low, that is, several orders of magnitude less than that of semiconductors. The fact that these substances have greater resistance than ferromagnetic materials results in much smaller induced currents in the material when alternating fields are applied.

Ferrites are ceramic materials with the general chemical formula $MOFe_2O_3$, where MO is one or more divalent metal oxides blended with 48 to 60 mole percent of iron oxide. Iron oxide magnetite (Fe_3O_4), nickel-zinc ferrite $(NiZnFe_2O_4)$, manganese-zinc ferrite $(MnZnFe_2O_4)$, and nickel ferrite $(NiFe_2O_4)$ are examples of this class of materials.

The magnetic moment of a substance or ion depends on the number of unpaired electrons and is equal to $\sqrt{n(n+2)}$, where n is the number of unpaired electrons. The ions with the greatest number of unpaired electrons, that is, Mn^{2+} and Fe^{3+}, have the highest magnetic moments.

Manganese-zinc ferrites have the highest relative permeabilities, μ_r, and exhibit volume sensitivities ranging from one hundred to several thousand ohm-centimetre. They are used in tuned circuits and magnetic power designs from the low kilohertz range into the broadcast spectrum.

Manganese ferrite is uniquely suited for applications as multiple output controls in switch-mode power supplies and high frequency magnetic amplifiers.

2.2.2.6 Super-paramagnetic materials

Super-paramagnetic materials are composed of an assemblage of ferromagnetic particles in a non-ferromagnetic matrix. One important example is the magnetic tape used in audio or video tape recorders.

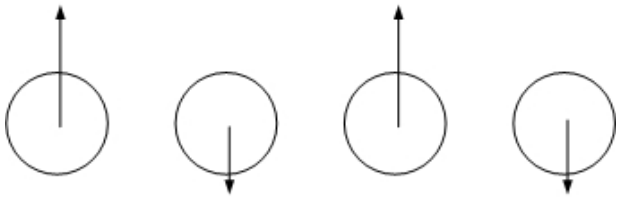

Figure 2.6: Structure of spin magnetic moment under an applied magnetic field in ferrimagnetic material

2.2.3 Complex relative permeability

The magnetic permeability μ of a medium at any point is defined as the magnetic field per unit magnetising field $(\frac{B}{H})$, with B the magnetic field and H the magnetising field. μ represents the extent to which a medium is permeable by a magnetic field. The relative permeability $(\mu = \mu_0\mu_r)$ of a medium is defined as the fraction increase in the field with respect to the field in free space when a material medium is introduced.

The relative complex permeability of magnetic material $(\mu_r = \mu_r^{'} - j\mu_r^{''})$ can be described by the following frequency dispersion equation [27]:

$$\mu_r = 1 + \frac{K}{1 + j\frac{f}{f_m}} = \frac{(K+1) + (\frac{f}{f_m})^2 - j(\frac{Kf}{f_m})}{1 + (\frac{f}{f_m})^2} \tag{2.47}$$

With $K = \frac{\mu_i}{\mu_0} - 1$ and μ_i the relative permeability at dc, also referred to as the initial permeability, and f_m the relaxation frequency, also referred to as the matching frequency, the real and imaginary parts of the permeability can be written as:

$$\mu_r^{'} = \frac{(K+1) + (\frac{f}{f_m})^2}{1 + (\frac{f}{f_m})^2} \tag{2.48}$$

and

$$\mu_r'' = \frac{(\frac{Kf}{f_m})}{1+(\frac{f}{f_m})^2} \tag{2.49}$$

The matching frequency f_m, is the frequency where the normalised input intrinsic impedance of the material becomes unity. For $f = f_m$:

$$\mu_r' = \frac{(K+2)}{2} \tag{2.50}$$

and

$$\mu_r'' = \frac{K}{2} \tag{2.51}$$

At high frequencies $\frac{\sigma}{\omega\varepsilon} << 1$ for a lossy magnetic material. The propagation constant in equation (2.30) may be expanded by the binomial theorem $(1+x)^n = 1+nx+\frac{n(n-1)}{2!}x^2+\frac{n(n-1)(n-2)}{3!}x^3+\cdots$ where $|x|<1$ and $x=-j\frac{\sigma}{\omega\varepsilon}$:

$$\gamma = j\omega\sqrt{\mu\varepsilon}\left[1-j\frac{\sigma}{2\omega\varepsilon}+\frac{1}{8}\left(\frac{\sigma}{\omega\varepsilon}\right)^2+\cdots\right] \approx \frac{\sigma}{2}\sqrt{\frac{\mu}{\varepsilon}}+j\omega\sqrt{\mu\varepsilon}\left[1+\frac{1}{8}\left(\frac{\sigma}{\omega\varepsilon}\right)^2\right] \tag{2.52}$$

The complex intrinsic impedance of the material in equation (2.31) can be simplified in a similar way:

$$\eta \approx \sqrt{\frac{\mu}{\varepsilon}}\left[1-\frac{3}{8}\left(\frac{\sigma}{\omega\varepsilon}\right)^2+j\frac{\sigma}{2\omega\varepsilon}\right] = \sqrt{\frac{\mu}{\varepsilon}}\left(1+j\frac{\sigma}{2\omega\varepsilon}\right) \tag{2.53}$$

At high frequencies, the complex intrinsic impedance in equation (2.53) will become $\sqrt{\frac{\mu}{\varepsilon}}$ and, from equation (2.52), $\beta = \omega\sqrt{\mu\varepsilon}$ for low values of σ.

2.2.4 Complex relative permittivity

The complex permittivity ε_r relative to free space ε_0 for a planer sample of lossy magnetic material in free space is defined as:

$$\varepsilon_r = \varepsilon_r^{'} - j\varepsilon_r^{''} = \varepsilon_r^{'}(1 - jtan\delta) \tag{2.54}$$

With $\delta = \frac{\sigma}{\omega\varepsilon}$ being the loss-tangent, if the scattering parameters S_{11} and S_{21} are measured in free space for a normally incident plane wave, the reflection and transmission coefficients, Γ and T, are related in the following equations [43] and [44]:

$$S_{11} = \frac{\Gamma\left(1 - T^2\right)}{1 - \Gamma^2 T^2} \tag{2.55}$$

and

$$S_{21} = \frac{T\left(1 - \Gamma^2\right)}{1 - \Gamma^2 T^2} \tag{2.56}$$

With

$$\Gamma = \frac{(\eta_n - 1)}{(\eta_n + 1)} \tag{2.57}$$

and

$$T = e^{-\gamma d} = |T|\, e^{j\phi} \tag{2.58}$$

$\eta_n = \sqrt{\frac{\mu_r}{\varepsilon_r}}$ is the normalised intrinsic impedance of the material.
The Γ and T can be written as:

$$\Gamma = A \pm \sqrt{A^2 - 1} \tag{2.59}$$

where

$$A = \frac{(S_{11}^2 - S_{21}^2) + 1}{2S_{11}} \tag{2.60}$$

and

$$T = \frac{S_{11} + S_{21} - \Gamma}{1 - (S_{11} + S_{21})\Gamma} \tag{2.61}$$

The plus and minus sign in equation (2.59) is chosen such that $|\Gamma| < 1$. The relative complex permittivity and relative complex permeability of the material can now be determined by:

$$\varepsilon_r = \frac{\gamma}{\gamma_0}\left(\frac{1-\Gamma}{1+\Gamma}\right) \tag{2.62}$$

and

$$\mu_r = \frac{\gamma}{\gamma_0}\left(\frac{1+\Gamma}{1-\Gamma}\right) \tag{2.63}$$

With $\gamma_0 = \left(\frac{j2\pi}{\lambda_0}\right)$ the propagation constant in free space and λ_0 the free-space wavelength, the propagation constant γ is given by:

$$\gamma = \frac{\left[log\left(\frac{1}{|T|}\right)\right]}{d} + j\left[\frac{2\pi n - \phi}{d}\right] \tag{2.64}$$

With $n = 0, \pm1, \pm2, \pm3, \cdots$ and with the material thickness d chosen such that $d < \lambda_m$, then ε_r and μ_r will have unique values corresponding to $n = 0$. $\lambda_m = \frac{\lambda_0}{\sqrt{\mu_r \varepsilon_r}}$ is the wavelength in the material. Consequently for $d > \lambda_m$, μ_r and ε_r can be determined by making measurements with two different material thicknesses.

2.2.5 Shielding effectiveness

When an EMW is a normal incident wave on a material, as shown in Figure 2.7, a part of the incident wave's (E_i) energy is reflected (E_r) by the first interface of the material and the remaining part (E_A) is absorbed and penetrates into the material [64]. The reflection is therefore partial. The absorbed energy that propagates toward the second interface is attenuated along the path. On the second interface of the material a part of the absorbed field is reflected back (E_M) toward the first interface. This is an internal reflection. The last part of energy $(E_{t)}$ is transmitted toward the outside of the material through the second interface. This phenomenon is called the shielding of an EMW.

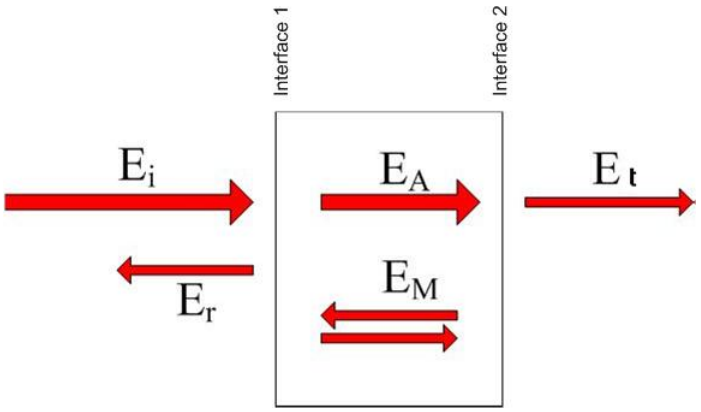

Figure 2.7: Propagation of an EMW through a shield

EMW shielding refers to the reflection and attenuation of EMWs by a material that acts as a reflector and attenuator in order to shield against penetration into and transmission through the material [22]. Shielding effectiveness (SE) is a measure of the capability of the shielding material to reflect and attenuate an incident EMW.

In order to reflect an EMW, the material must have mobile charge carriers in the form of electrons and holes which interact with the electromagnetic field. The material tends to be electrically conducting, although a high conductivity (σ) is not required. Metals are by far the most common materials for reflection owing to the free electrons in them. Reflection is a result of a mismatch between the incident wave impedance and the input intrinsic impedance of the material. For the EMW to be completely absorbed by the material, the input intrinsic impedance of the material should be equal to the incident wave impedance (zero reflection).

For the material to attenuate the absorbed propagating EMW internally, the material should have electric and magnetic dipoles that interact with the electromagnetic fields. The electric dipoles may be provided by material with high values of dielectric constants (permittivity), while the magnetic dipoles may be provided by material with high values of magnetic permeability.

Multiple reflections and attenuation internal to the material also contribute to the SE of the material [23]. This contribution can be disregarded for material thickness that is much greater than the skin depth of the material. The skin depth, or depth of penetration, is the distance the EMW is propagated in the material when it is attenuated by $e^{-1} = 0.368$ of its initial field strength.

For the purpose of explanation, let E^i and H^i be the incident fields, E^t and H^t the transmitted fields, and E^r and H^r the reflected fields. For a planer sheet of lossy composite magnetic material with thickness d in free space, let the first interface from free space to the material that the fields will encounter at $z = 0$ be interface 1; the second interface from the material to free space at $z = d$ be interface 2; and the interface from the material to free space that the internal reflected fields will encounter at $z = 0$ be interface 3; and so on for multiple internal reflections.

From equation (2.38) at interface 1:

$$E_1^i + E_1^r = E_1^t \tag{2.65}$$

and

$$H_1^i + H_1^r = H_1^t \tag{2.66}$$

From equations (2.28) and (2.29) the following relationships exist:

$$E_1^i = \eta_0 H_1^i \tag{2.67}$$

and

$$E_1^r = -\eta_0 H_1^r \tag{2.68}$$

and

$$E_1^t = \eta H_1^t \tag{2.69}$$

From equations (2.65), (2.66), and (2.67) to (2.69):

$$E_1^i + E_1^r = \eta H_1^t \tag{2.70}$$

and

$$\frac{E_1^i}{\eta_0} + \left(\frac{-E_1^r}{\eta_0}\right) = H_1^t \tag{2.71}$$

The reflection coefficient for the electric field strength at interface 1 can now be determined from equations (2.70) and (2.71):

$$\Gamma_1^E = \frac{E_1^r}{E_1^i} = \frac{\eta - \eta_0}{\eta_0 + \eta} \tag{2.72}$$

From equations (2.65), (2.66), and (2.67) to (2.69):

$$H_1^i + H_1^r = \frac{E_1^t}{\eta} \tag{2.73}$$

and

$$\eta_0 H_1^i + (-\eta_0 H_1^r) = E_1^t \tag{2.74}$$

The reflection coefficient for the magnetic field strength at interface 1 can now be determined from equations (2.73) and (2.74):

$$\Gamma_1^H = \frac{H_1^r}{H_1^i} = \frac{\eta_0 - \eta}{\eta_0 + \eta} \tag{2.75}$$

Using equations (2.65) to (2.69) the transmission coefficients T^E and T^H can also be found at interface 1:

$$T_1^E = \frac{E_1^t}{E_1^i} = \frac{2\eta}{\eta_0 + \eta} \tag{2.76}$$

and

$$T_1^H = \frac{H_1^t}{H_1^i} = \frac{2\eta_0}{\eta_0 + \eta} \tag{2.77}$$

A similar approach will lead to the reflection and transmission coefficients at interface 2:

$$\Gamma_2^E = \frac{E_2^r}{E_2^i} = \frac{\eta_0 - \eta}{\eta_0 + \eta} \tag{2.78}$$

$$\Gamma_2^H = \frac{H_2^r}{H_2^i} = \frac{\eta - \eta_0}{\eta_0 + \eta} \tag{2.79}$$

$$T_2^E = \frac{E_2^t}{E_2^i} = \frac{2\eta_0}{\eta_0 + \eta} \tag{2.80}$$

$$T_2^H = \frac{H_2^t}{H_2^i} = \frac{2\eta}{\eta_0 + \eta} \tag{2.81}$$

By definition [65], the SE is the ratio of the signal received (from a transmitter) without the shield to the signal received with the shield; the insertion loss occurs when the shield is placed between the transmitting antenna and the receiving antenna. A theorectical model of the reflection and multiple internal reflections of an EMW propagation through material is developed in [3]. The well-known and generally used Schelkunoff model [66] of SE is determined by the reflection loss (R), attenuation (A), and the loss resulting from the multiple internal reflections (M), and can be determined by:

$$SE_{dB} = R + A + M \tag{2.82}$$

The total reflection loss (R) is by definition:

$$R = -20log|T| \tag{2.83}$$

Where (T) is the nett transmission coefficient across the two mismatched interfaces and is the product of the transmission coefficient at each interface:

$$T = \frac{2\eta_0}{\eta_0+\eta}\frac{2\eta}{\eta_0+\eta} = \frac{4\eta_0\eta}{(\eta_0+\eta)^2} \tag{2.84}$$

Whith η_0 the intrinsic impedance of free space and η the intrinsic impedance of the material. The attenuation across the shielding material with thickness (d) is [3]:

$$A = 20log\left|e^{\alpha d}\right| \tag{2.85}$$

With γ the propagation constant, the loss resulting from multiple internal reflections and attenuations in the material is [3]:

$$M = 20log\left|1-\Gamma e^{-2\gamma d}\right| \tag{2.86}$$

Where the nett reflection coefficient (Γ) across the two mismatched interfaces is the product of the reflection coefficients at each interface $\frac{(\eta_0-\eta)(\eta-\eta_0)}{(\eta_0+\eta)^2}$.

It is concluded in [3] that equations (2.83) and (2.85) do not satisfy the laws of physics related to reflection, transmission and absorption, and the following equations were obtained with an iterative algorithm that satisfies the conservation laws:

$$R = -20log\left|\Gamma\frac{e^{2\gamma d}-1}{e^{2\gamma d}-\Gamma^2}\right| \tag{2.87}$$

$$A = -20log\left|(1-\Gamma)(1-e^{-\gamma d})\frac{e^{\gamma d}}{e^{\gamma d}-\Gamma^2}\right| \tag{2.88}$$

2.3 ABSORBER AND SHIELDING MATERIAL

The shielding phenomenon is a combination of reflection from interface 1 given by equation (2.83), internal attenuation given by equation (2.85), and multiple internal reflections and attenuations inside the shielding material given by equation (2.86) as shown in Figure 2.7. Various constructions of building material can be developed that use one of these mechanisms to achieve a required SE. Concrete has been used as a building material for many years, and has good mechanical properties and durability for construction. Although it is slightly conductive, concrete is a poor EMW shielding material [67]. To improve the SE of concrete and cement-based material, various materials can be added to its matrix as fillers.

2.3.1 Building material as absorbers and shields

Owing to its wide application and low cost, concrete and cement-based material offers an inexpensive solution as host for a shield against EMW propagation for protection against electromagnetic pollution and environmental electromagnetic security.

2.3.1.1 Material for reflection

There are three main types of conductive filler used in cement matrix materials; these are conductive polymers, carbon materials and metal materials.

Conductive paint is a popular shielding method because it can be processed easily and is cost-effective. Water-based paints are used widely with metal powders with high conductivity, but the dispersed metal particles are easily oxidised [37]. However, there is

a need for new fillers that are lightweight, chemically stable and more easily adapted to a wide range of environments. Multi-walled carbon nanotubes are one such filler owing to their excellent electrical and mechanical properties and unique structure. The SE achieved by this filler is mainly as a result of reflection, because of the high conductivity of the carbon.

Conductive cement-based material can be produced by using carbon fibre, steel fibre or lead as conductive fillers [59]. The SE increases with an increase in the conductivity and thickness of the cement-based material. With $\sigma > 0.1 S/m$ the SE increases significantly. In order for a conductive filler to be highly effective for shielding, it should preferably have a small unit size, a high conductivity and a high aspect ratio. The curing time for the cement-based material should be more than 20 days, as the reflection coefficient only stabilises after that time [68]. Carbon fillers include graphite, carbon black, coke and carbon fibre. Bamboo-charcoal [12] used as replacement for the fine aggregate of cement mortar will increase the SE of the mortar by up to 90%. A filling of carbon black (CB) improves the dielectric constant and the loss factor of cement-based material remarkably [14].

Reinforced walls show an SE of 5 to 8 dB in the GSM frequency bands. This type of shield also relies on reflection and is not cost-effective or practically applicable in many circumstances [17].

2.3.1.2 Material for internal multiple reflections

Owing to the electromagnetic transparency of expanded polystyrene (EPS), the cement-based composites filled with EPS beads can be regarded as a type of porous material [6]. The 1 mm spherical polystyrene beads create cavities in the cement-based material which increases the multiple internal reflections.

2.3.1.3 Material for attenuation

Only by using EMW absorbing materials and transferring the electromagnetic energy to other forms of energy, can the EMI radiation be attenuated to the furthest extent. EMW

attenuation material can be divided into three types, that is electric loss, magnetic loss and dielectric loss materials. Conductive materials are electric attenuation absorbents, ferrites are magnetic loss absorbents and many ceramic materials, such as barium titanate, are dielectric loss absorbents.

2.3.2 Conclusion

Concrete and cement-based building material is the material used most for building in southern African countries. It is one of the oldest and most widely used construction materials in the world and benefits the owner, developer and designer, as it is versatile, has aesthetic appeal, is cost-effective and is easily available. Its strength, durability and natural thermal mass result in buildings requiring low maintenance and having high operating energy efficiency [69].

Table 2.2 gives a summary of the various research contributions to increase the SE in cement-based material.

Composite Material	Contribution	Referance
MnZn	The inclusion of silica fume can improve the impedance matching between the MnZn cement-based composite (CBCC) and free space.	[50]
MnZn and NiZn	The dielectric loss in *NiZn* and *MnZn* composite ferrites can be increased by the inclusion of conducting particles such as carbon in the mixture.	[28] and [30] [26] and [27]
MnZn wood	A wooden panel is manufactured by sandwiching MnZn ferrite powder between thin wooden layers.	[32] and [9]
Bamboo charcoal	The use of bamboo charcoal that has electric conductivity effectively improves the SE of CBCC.	[70]
Carbon black (CB)	A filling of CB improved the dielectric constant and loss factor of CBCC.	[14]
Conductive cement	Mixing conductive components such as carbon fibre, steel fibre and lead improves the conductivity and SE of CBCC.	[59]
PVC	PVC polymer-based composites with different types of single ferrite fillers were examined.	[35] and [36]
Graphite fibre	Several guidelines on material applications were presented and discussed for EMC testing and practical application.	[51]
EPS	Creating small cavities in the cement mortar by adding small (1 mm) EPS spheres to the mixture increased the SE of the material.	[6]

Table 2.2: Contributions to research in cement-based composite materials

CHAPTER 3

METHODOLOGY

3.1 SIMULATION

3.1.1 MatLab simulation

The SE can be calculated from equations (2.82) to (2.85) and presented graphically. The propagation path through the material can be represented as a transmission line [71].

3.1.1.1 Transmission line model of a shield

There is a direct analogy between a uniform transmission line and a uniform plane wave travelling through a medium. The field distributions for a plane wave and a transmission line are both known as transverse electromagnetic waves (TEM) because $\boldsymbol{E}$ and $\boldsymbol{H}$ are both perpendicular to the direction of propagation, and both lie in the transverse plane. However, in transmission lines it is customary to define a voltage and a current.

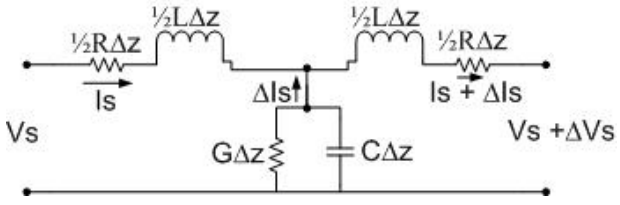

Figure 3.1: RLCG transmission line model

The circuit model in Figure 3.1 contains the inductance (L), capacitance (C), shunt conductance (G), and series resistance (R) associated with an incremental length (Δz) of line. The series elements are divided in half to produce a symmetrical network because the section of the transmission line looks the same from either end. The voltage equation around the perimeter of the circuit in Figure 3.1 is:

$$V_s = \left(\frac{1}{2}R\Delta z + j\frac{1}{2}\omega L\Delta z\right) I_s + \left(\frac{1}{2}R\Delta z + j\frac{1}{2}\omega L\Delta z\right)(I_s + \Delta I_s) + (V_s + \Delta V_s) \tag{3.1}$$

and

$$\frac{\Delta V_s}{\Delta z} = -(R + j\omega L) I_s - \left(\frac{1}{2}R + j\frac{1}{2}\omega L\right)\Delta I_s \tag{3.2}$$

As Δz approaches zero, ΔI_s also approaches zero, and the second term on the right vanishes; hence equation (3.2) becomes:

$$\frac{dV_s}{dz} = -(R + j\omega L) I_s \tag{3.3}$$

From the voltage across the shunt branch:

$$\frac{dI_s}{dz} = -(G + j\omega C) V_s \tag{3.4}$$

By comparing equations (3.3) and (3.4) with equations (2.26) and (2.27), an analogy between G and σ, C and ε, and L and μ can be indentified. There is no analogy, however, for the conductor resistance per unit length R. The value for R in the circuit equation can be obtained by replacing $j\omega\mu$ by $(R + j\omega L)$. When ferrite materials enter the field problem, a complex permeability $\mu = \mu' - j\mu''$ is used to include the effect of non-ohmic losses in

that material. Under these conditions $\omega\mu''$ is analogous to R and μ' to L. These primary parameters are frequency dependent.

The voltage that propagates in the $+z$ direction is $V_s = V_0 e^{-\gamma z}$ and thus the propagation constant in equation (2.30) becomes

$$\gamma = \alpha + j\beta = \sqrt{(R + j\omega L)(G + j\omega C)} \tag{3.5}$$

The wavelength is defined as the distance that provides a phase shift of 2π radians ($\lambda = \frac{2\pi}{\beta}$), and the phase velocity is $\upsilon = \frac{\omega}{\beta}$. The characteristic impedance Z_0 is analogous to η:

$$Z_0 = \sqrt{\frac{R + j\omega L}{G + j\omega C}} \tag{3.6}$$

and the reflection coefficient for a line terminated in a load Z_L is:

$$\Gamma = \frac{Z_L - Z_0}{Z_L + Z_0} \tag{3.7}$$

From equation (2.46), the input impedance can also be written as:

$$Z_{in} = Z_0 \frac{Z_L + Z_0 tanh\gamma d}{Z_0 + Z_L tanh\gamma d} \tag{3.8}$$

The primary parameters can be found by using (3.5) and (3.6) at a specific frequency:

$$R + j\omega L = Z_0\gamma = \eta\gamma \tag{3.9}$$

and

$$G + j\omega C = \frac{\gamma}{Z_0} = \frac{\gamma}{\eta} \tag{3.10}$$

In the transmission line modelling of the shield, the permeability is calculated from equations (2.48) and (2.49). The relative permittivity ε_r is assumed to be constant at $7Fm^{-1}$. The propagation constant and intrinsic impedance are calculated from equations (2.30) and (2.31) respectively. The series and shunt impedances are calculated from equations (3.9) and (3.10) in order to find the primary parameters R, L, C, and G for a 25 mm thick shield. The transmission line model with series and shunt components and with operating parameters Z_L, Z_S set to 377Ω, is then analysed from 800 MHz to 2.8 GHz according to the ICASA frequency band allocations in Table 3.3 and the scattering parameters S_{11} and S_{21} determined with Matlab. Table 3.1 summarises the parameters used for the transmission line model. The reflection coefficient and the transmission coefficient are calculated and plotted on a graph including the SE as shown in Figure 3.2.

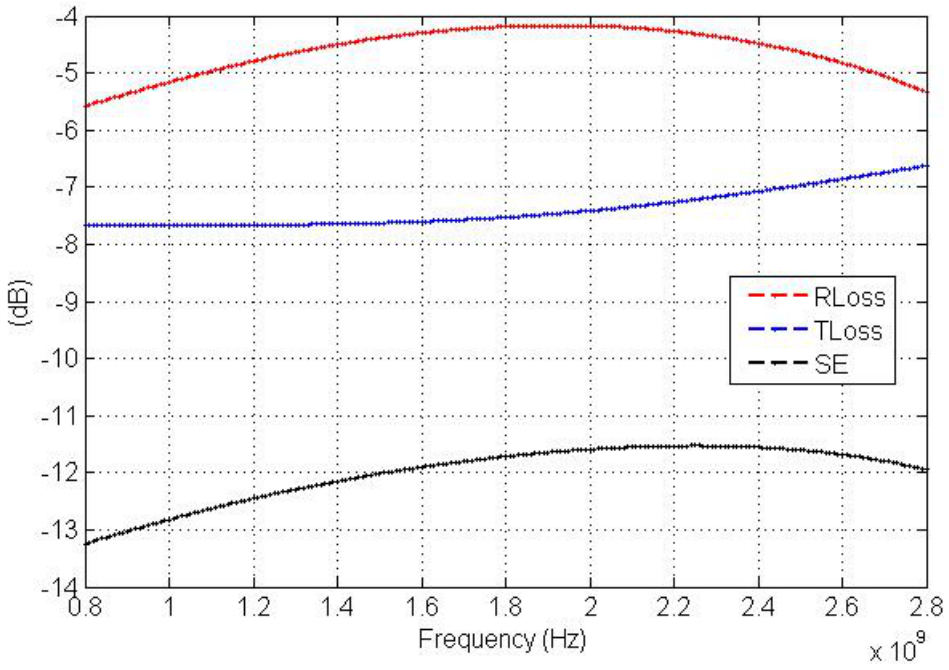

Figure 3.2: Reflection loss, transmission loss and SE of the transmission line model

Parameter	Symbol	Value
Relative permittivity	ε_r	$7Fm^{-1}$
Permittivity	ε	$8.854x10^{12}\varepsilon_r$
Conductivity	σ	$0.5Sigma$
Initial permeability	K	$10Hm^{-1}$
Matching frequency	f_m	$30MHz$
Frequency	f	$800MHz$ to $2.8GHz$
Length	z	$25mm$
Relative permeability (real)	$\mu_r^{'}$	$\frac{(K+1)+(\frac{f}{f_m})^2}{1+(\frac{f}{f_m})^2}$
Relative permeability (imaginary)	$\mu_r^{"}$	$\frac{(\frac{Kf}{f_m})}{1+(\frac{f}{f_m})^2}$
Relative permeability	μ_r	$\mu_r^{'} - j\mu_r^{"}$
Permeability	μ	$\mu_0\mu_r$
Intrinsic impedance	η	$\sqrt{\frac{j\omega\mu}{\sigma+j\omega\varepsilon}}$
Attenuation constant	α	$(\frac{\sigma}{2})(\sqrt{\frac{\mu}{\varepsilon}})$
Phase constant	β	$\left\lvert j2\pi f\sqrt{\mu\varepsilon}\right\rvert$
Propagation constant	γ	$\alpha + j\beta$
Series impedance	$R + j\omega L$	$\eta\gamma$
Shunt impedance	$G + j\omega C$	$\frac{\gamma}{\eta}$

Table 3.1: Summary of the parameters used for the transmission line model

In Figure 3.2 it is evident that with the chosen parameters of typical magnetic material, the transmission loss is higher than the reflection loss. The transmission loss indicated is a combination of the attenuation and internal multiple reflections and attenuations of the transmission line. The reflection loss is the total loss resulting from reflection at the input port of the transmission line.

3.1.1.2 Mathematical simulation

The propagation of the plane wave through the composite magnetic material can be simulated by using equations (2.82) to (2.86). Figure 3.3 shows the mathematical simulation of the SE, transmission loss and reflection loss for the frequency band allocations by ICASA, as indicated in Table 3.3. The same material parameters are chosen as for the transmission line model summarised in Table 3.2. The mathematical model show results in Figure 3.3 similar to those of the transmission line model in Figure 3.2.

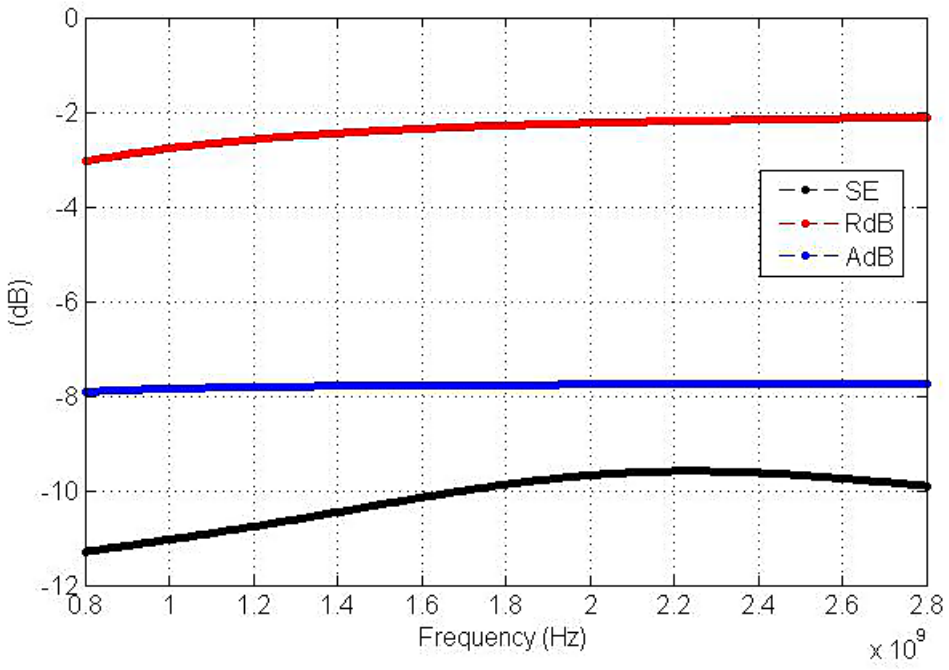

Figure 3.3: Shielding effectiveness, reflection loss and transmission loss plot from mathematical simulation

Parameter	Symbol	Value
Relative permittivity	ε_r	$7Fm^{-1}$
Permittivity	ε	$8.854x10^{12}\varepsilon_r$
Conductivity	σ	$0.5Sigma$
Initial permeability	K	$10Hm^{-1}$
Matching frequency	f_m	$30MHz$
Frequency	f	$800MHz$ to $2.8GHz$
Material thickness	d	$25mm$
Relative permeability (real)	$\mu_r^{'}$	$\frac{(K+1)+(\frac{f}{fm})^2}{1+(\frac{f}{fm})^2}$
Relative permeability (imaginary)	$\mu_r^{"}$	$\frac{(\frac{Kf}{fm})}{1+(\frac{f}{fm})^2}$
Relative permeability	μ_r	$\mu_r^{'}-j\mu_r^{"}$
Permeability	μ	$\mu_0\mu_r$
intrinsic impedance	η	$\sqrt{\frac{j\omega\mu}{\sigma+j\omega\varepsilon}}$
Attenuation constant	α	$(\frac{\sigma}{2})(\sqrt{\frac{\mu}{\varepsilon}})$
Phase constant	β	$\left\lvert j2\pi f\sqrt{\mu\varepsilon}\right\rvert$
Propagation constant	γ	$\alpha+j\beta$
Attenuation loss	A	$-20Log(\lvert e^{-\gamma z}\rvert)$
Reflection loss	R	$-20Log(\left\lvert\frac{4\eta_0\eta}{(\eta_0+\eta)^2}\right\rvert)$
Multiple internal att. and refl.	M	$20Log(\left\lvert 1-(\frac{(\eta_0-\eta)^2}{(\eta_0+\eta)^2})e^{-2\gamma d}\right\rvert)$
Shielding effectiveness	SE	$R+A+M$

Table 3.2: Summary of the parameters used for the mathematical model

3.2 PREPARATION OF SAMPLES

The composite cement-based samples as shown in Figure 3.4 were prepared in square tile format with 300 mm side lengths and a thickness of 25 mm. The mixture for the plaster cement comprised of one part cement and six parts sifted river sand. The research mixture used consisted of one part cement, x parts river sand and y parts ferrimagnetic or magnetic powder with $x + y = 6$. The ferrimagnetic powder is Mn-Zn-ferrite with an initial relative complex permeability of 13000 H/m and the magnetic powder is MnO_2 [20].

Figure 3.4: Example of a 25 x 300 x 300 mm composite plaster cement test sample

The composite mixture was mixed well while still dry to ensure a homogeneous result. Water was replaced with Bond-it [72], a liquid cement adhesive, to strengthen the bonding of the composite material. After the the bonding liquid was added the mixture was well mixed again. The mixture was then poured into the wooden tile moulds and compressed to ensure

all air pockets were removed. The prepared samples were cured naturally for at least 12 weeks to reduce the moisture content, as moisture increases the conductivity of the material, hence increasing reflection loss and SE [73].

3.2.1 Cement and building sand

Portland cement [74] is a common cement type used internationally. It is a fine powder produced by 90% ground Portland cement clinker, a limited amount of calcium sulphate and up to 5% minor constituents. In terms of mass, Portland cement clinker consists of at least 67% calcium silicates $(3CaOSiO_2)$ or $(2CaOSiO_2)$ and aluminium and iron phases.

Building sand is a naturally occurring granular material. It is composed of finely ground rock and mineral particles. The most common constituent of sand is silica (silicon-dioxide) or SiO_2. Sand grains range in diameter from 62.5 μm to 2 mm.

3.2.2 Magnetic powder

Electrolytic manganese dioxide (EMD), MnO_2, was used as magnetic powder. It is produced for alkaline and lithium primary chemistry and cylindrical and flat cells. It has a density of 23 $g/inch^3$.

3.2.3 Ferrimagnetic powder

The ferrimagnetic powder used to prepare the samples was manganese-zinc ferrite $MnZnFe_2O_4$. Two variations were investigated: $CHY5K$ ferrite with an initial permeability of 5000 H/m and $CHY13K$ with an initial permeability of 13000 H/m. This powder has a density of $1.3g/cm^3$ to $1.5g/cm^3$.

3.2.4 Curing time

A measuring system was developed by [75] to determine the scattering parameters for evaluating fresh cement samples for quality purposes. The study shows a decrease in the reflection

coefficient and an increase in the transmission coefficient with increasing curing time. The reflection coefficient of cement-based material was measured by [68] to determine the presence of chloride, which is the main contributor to corrosion in reinforced concrete. Measurements showed that the reflection coefficient stabilised after 20 days of curing in a 200 mm thick sample. The moisture content of the sample has a direct influence on the dielectric properties of the sample material. Similar results were found by [73] for a 150 mm thick mortar (plaster cement) mixture. It was found that the real part of the permittivity remained constant but the imaginary part decreased with curing time.

3.3 MEASUREMENT SETUP

3.3.1 Measurement techniques

Although the shielding of the EMW mechanism is a fixed system, the determination of SE can be conducted in various ways. All the methodologies followed in the literature to determine SE measure the scattering parameters S_{11} and S_{21}, and then use the reflection loss and transmission loss calculated from the scattering parameters to find SE. The variation is found in the method of measuring the scattering parameters.

The standard method for measuring the effectiveness of the electromagnetic shielding of enclosures is given by [65]. The applicable frequencies for which SE can be determined are divided into three distinct ranges, low range (9 kHz-16 MHz), resonant range (20-300 MHz), and high range (300 MHz-18 GHz). Signals used for measurements in the high frequency range are planer and of the continuous wave (CW) type. Dipoles, biconical antennae, horns, yagis, log periodic, or other linear antenna types have to be used. The reference measurement is done with antennae at least 2 m apart but the maximum available separation has to be used. The largest receiver response has to be recorded to determine the minimum SE. The separation distance between the two antennae should be recorded and the height of both antennae should be approximately the same. The positioning of the transmitting antenna should be outside the shield (anechoic chamber) and the receiving antenna inside the shield. The transmitting antenna should be positioned at least 1.7 m from

the test surface. A minimum spacing of 0.3 m from the shielding surface to the closest point of the receiving antenna should be maintained.

It is also stated by [65] that when testing in non-anechoic enclosed locations, it is good practice to establish a baseline reference response curve for that location without the DUT present. If this cannot be done, comparable DUT data acquired in an ideal test location may be used. A field penetrating a shielding material arises from both the electric and magnetic components of the electromagnetic energy incident upon the shield. Separate measurements of the electric and magnetic fields demonstrates that they are functions of the incident wave. SE can be expressed in electric field terms and is given by the following equation:

$$SE = 20log_{10}\frac{|E_1|}{|E_2|} \tag{3.11}$$

where E_1 is the electric field measured at the receiving antenna without the DUT between the antennae and E_2 is the electric field measured at the receiving antenna with the DUT between the antennae. One can express SE in power terms and it can be written as:

$$SE = 10log_{10}\frac{P_1}{P_2} \tag{3.12}$$

where P_1 is the power detected in the absence of the DUT, and P_2 is the power detected when the DUT is present.

A 20D shorted coaxial waveguide with diameters of 8.66 and 19.94 mm for the inner and outer conductors respectively was used by [76] to determine the reflection coefficient between 1 and 4 GHz, by mounting the cylindrical shield in the waveguide.

Reflection measurements have been performed by [40] in an anechoic chamber with the setup based on a monostatic configuration. This consisted of four similar horn antennae

which were positioned in front of the material sample for normal incidence 3 m away from the sample. The antenna array allowed for measurements of different states of polarisation, using a *HP*8510*B* VNA.

The location of the antennae is instrumental in the accuracy of measurements. A problem could arise when it becomes nessary to determine the SE of a material if the anechoic chamber is constructed of the same material as it is too expensive and time consuming to re construct the whole chamber for accurate measurements. A similar problem can arise in the measurement of the SE of construction. A test system was produced using a coaxial flange for a frequency range of 9 kHz to 1 GHz by [22] and [34]. Accordingly, the shape and dimensions were calculated for a 50Ω system. The central conductor was manufactured from brass and the rest of the flange was made from aluminium alloy. The S_{11} and S_{22} scattering parameters were measured and found to be under -15 dB in the whole frequency range, while the S_{21} and S_{12} parameters were less than 1 dB in the frequency range. The composite concrete samples were manufactured in the shape of a thin (8 mm) ring which was inserted into the flange, and the S_{11} and S_{21} scattering parameters were measured to determine the SE. This method is also known as the coaxial line technique with an inserted coaxial cell to hold the sample. It is generally used to measure the permeability and permittivity of material.

A coaxial TEM cell similar to the flange was also used by [3] to measure the scattering parameters. As shown in Figure 3.5, an RF generator output was amplified (power and voltage) and transmitted through an attenuator to a dual directional coupler which fed the TEM cell in which the sample material was. The coupler allowed for the separation of the incident and the reflected waves. An oscilloscope showed the oscillations that were transmitted through the cell and a selective micro voltmeter measured the modules of the incident, reflected and transmitted waves.

The field strength with and without a shield was measured at different operating frequencies to determined the SE of a circular loop-shaped shield [77]. A hollow iron cylinder with a thickness of 1.2 mm and an inner diameter of 7.25 mm was placed coaxially around an

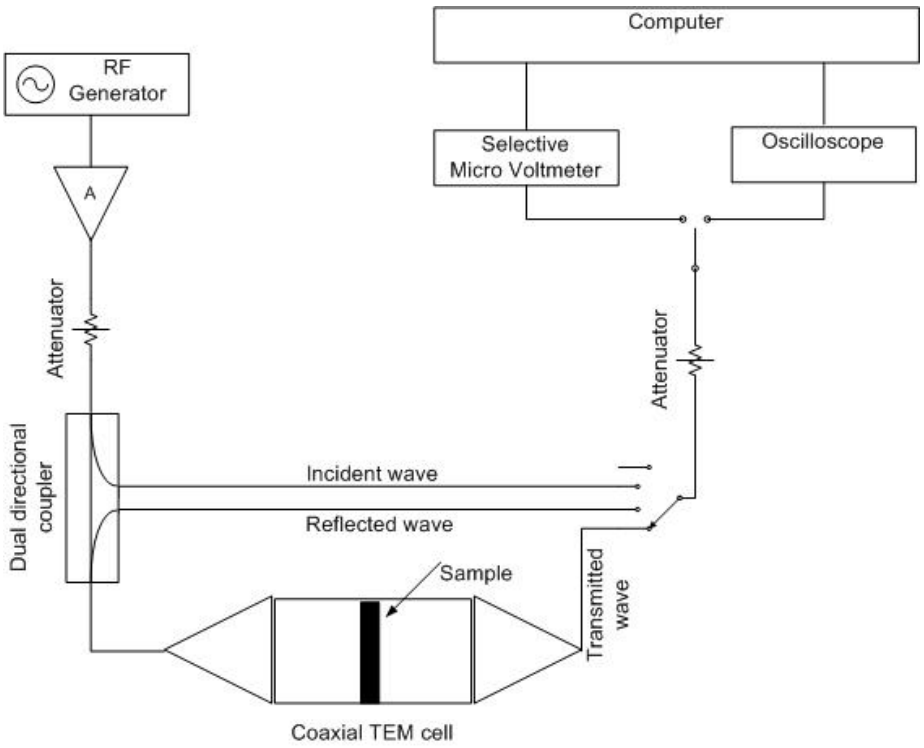

Figure 3.5: Measurement system with TEM cell by [3] to measure scattering parameters .

1.98 mm inner conductor and then bent to form a circular loop with an inner radius of 0.41 m. The shield was electrically closed at each end to complete the return path in order to ensure that the induced current could flow in the opposite direction to the primary current circulating in the inner conductor. The return path was the shield itself and it was assumed that two current sheets were flowing in opposite directions along the external and internal surfaces. The two currents were coaxial and the corresponding magnetic fields cancelled each other out, thus not altering the magnetic field distribution that was associated with the primary current. The measurement with and without the shield was achieved by connecting and disconnecting the inner and outer conductors of the shield loop ends. This methodology was only applied to audio frequencies.

A similar setup as in Figure 3.6 is the most widely used in research. This setup was used by [78] to measure the power received at the receiving antenna with and without the shield in the propagation path to determine the SE, but the receiving antenna was mounted in an aluminium box with a window that was the same size as the opening of the horn

antenna. This was to ensure that no microwave power leaked into the box by a path other than through the window. This was tested by covering the window with an aluminium plate while measuring the received power. The limitations of this setup were investigated by [79]. The required size of the samples and the distance between the antennae were investigated.

A shield box made from 3 mm thick copper was developed with two compartments by [80]. The two antennae were placed in the two compartments facing each other with the sample under test placed between the two compartments. In principle, this was similar to the widely used setup in Figure 3.6 and used to shield any noise coming from outside. It has, however, only been used for frequencies below 1 MHz.

The use of reverberation chambers in the measurement setup is a relatively new method for determining SE. The setup used by [81], [82] and [83] comprised a screened room or chamber with the addition of a metallic paddle or tuner situated anywhere in the chamber. The function of the paddle was to stir the modes inside the chamber to produce a superposition of multiple reflected waves which changed every time the paddle was rotated. This ensured a statistically uniform field inside the chamber. A smaller chamber with a window was placed inside the first chamber. The size of this nested chamber depended on the frequency range. The material to be tested was placed in the window and the receiving antenna was situated inside the nested chamber. This method is referred to as the nested reverberation chamber setup.

Measuring the S_{11} parameter to determine the reflection loss by a setup known as the NRL Arch technique (Naval Research Laboratory) is also a common method of specifying SE and has been used by [33]. In this study the antennae were localised in a reference arch manufactured from EMW transparent material used for aligning the two antennae at the same angle for both emission (incident angle) and reception (reflected angle). The reference plane was a conductive metal plate which was covered by the absorbing material. It was, however, shown by [84] that the reflection loss varies with variation in the incident and reflected angles. These vary from -13 dB at 10° to -6 dB at 60°. This makes the results achieved with the NRL Arch technique doubtful.

The SE measurement of a pulsed electric field system was made up of a electromagnetic pulse (EMP) source and a receiving device by [59]. The EMP source was a high voltage pulsed source which generated a puls of up to 30 kV and an electric field radiator (horn antenna). The receiving device consisted of a current probe, a fibre optic transmission system, a digital oscilloscope and a computer. The current probe was a monopole antenna. The fibre optic transmission system was composed of a light transmitter, a fibre optic cable and a light receiver. The received signals at the current probe were converted to light signals by the light transmitter, while the optic signals were transmitted to the light receiver through the fibre optic cable. The receiver transformed the optic signals into electrical signals in order for the digital oscilloscope to make the measurements.

3.3.2 Implemented measurement system

The measurement system implemented by the author is shown in Figure 3.6 and was also used by [4]. The arrangement was carried out using an Agilent Technologies $E5071C$ vector network analyser (VNA), and two ultra broadband open horn antennae. The transmitting (TX) antenna used was a 500 MHz to 4 GHz double-ridged horn antenna, part number 470523 from Saab-Grintek Technologies. The receiving (RX) antenna used was a model 3115 double-ridged waveguide horn antenna manufactured by ETS-Lindgren with a frequency range of 750 MHz to 18 GHz. Measurements were done in an anechoic chamber lined with Eccosorb AN absorption material operational for the frequency range 600 MHz to 40 GHz and designed to reflect less than -20 dB of normal incident energy. The test setup was calibrated to ensure minimum VSWR and path loss between the TX and RX antennae.

The TX antenna was positioned on the outside of the chamber on an adjustable antenna mount. This allowed the antenna position to be calibrated to ensure minimum volatge standing wave ratio (VSWR). The antenna was extended with the aid of an aluminium cone, lined on the inside with absorber material to guide the EMW into the chamber through a window in the chamber wall, as shown in Figure 3.7.

The RX antenna was installed inside the chamber. To ensure that the antennae were hori-

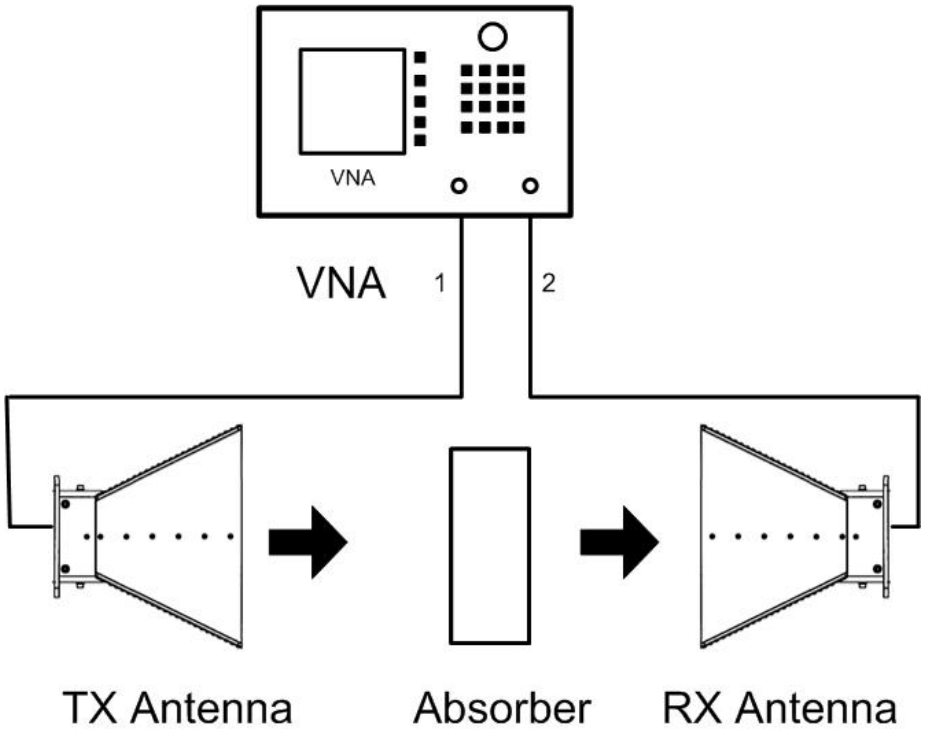

Figure 3.6: Measurement setup in anechoic chamber

zontally and vertically aligned, a lazer beam was used. The antennae were futher adjusted to ensure maximum power reception at the RX antenna during setup callibration.

3.3.2.1 ETS-Lindgren antenna

The ETS-Lindgren receiving antenna comprised a double-ridged waveguide horn antenna see Figure 3.8. The Model 3115 uses a Type N precision connector and accepts up to 500 Watt of continuous input power. The antenna high gain and low VSWR over its operating frequency translates into efficient amplifier use and higher field strengths. Model 3115 sweeps from 750 MHz to 18 GHz without stopping for band breaks, making it ideal for automated testing. The VSWR rating is 5 : 1 maximum and less than 2 : 1 above 800 MHz and it has a maximum continuous power output ability of 500 Watt. Figure 3.9 shows the antenna gain of the ETS-Lindgren antenna.

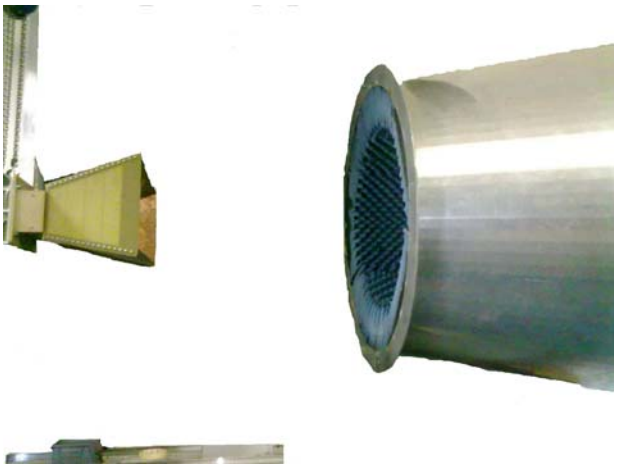

Figure 3.7: Transmit antenna setup for measurements

3.3.2.2 Saab-Grintek Technologies antenna

The transmitting antenna is shown in Figure 3.10 and is a Model 470523-00000 double-ridged horn antenna by Saab-Grintek Technologies and is suitable as a gain reference antenna for wide band measurements. It can also be used as a wide band source in anechoic chambers and compact ranges. It has a frequency range of 500 MHz to 4 GHz. The nominal gain is 10 dBi and it can handle 50 Watt power. The VSWR rating is less than 2.5 : 1. Figure 3.11 shows the antenna gain of the Saab-Grintek Technologies antenna.

3.3.3 Transmission loss measurement

The S_{21} scattering parameter was measured with the setup shown in Figure 3.6 to determine the transmission coefficient of the test samples. The transmission coefficient was calculated from equation (2.61).

3.3.4 Reflection loss measurement

In the measurement setup for the S_{11} scattering parameter, only the TX antenna and the VNA were used. The S_{11} parameter of a conductive plate with the same dimensions as the absorber material DUT was measured and used as a reference. The absorption and reflection loss of

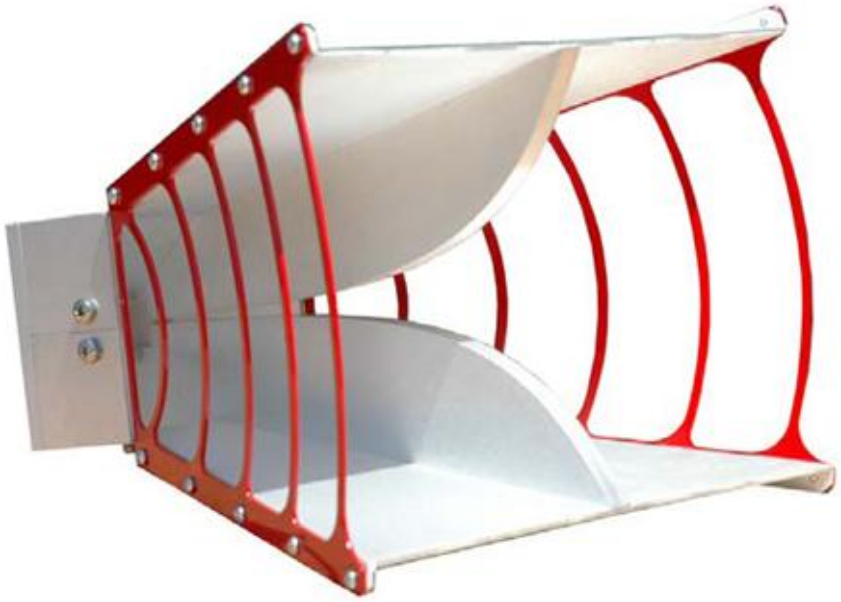

Figure 3.8: ETS-Lindgren antenna used as receive antenna

the material were then determined without a conductive back plate by measuring the S_{11} of the absorbing material. Traditional time domain reflectometry (TDR) measurement was made by launching an impulse or step into the test device and observing the response in time with a wide band receiver. The transformation made by the VNA resembles TDR. However, the VNA makes swept frequency response measurements, and mathematically transforms the data into a TDR-like display. This is useful for determining impedance mismatches, which are the main cause of reflection loss. This measurement yields the actual impedances and is available immediately from the VNA display. The gating function on the VNA allows the selective removal of reflection or transmission responses. The gate was set in the time domain the data was then converted to the frequency domain by means of a Fourier transformation. The gate centre position and time span or start and stop times were then set and the reflection coefficient determined from S_{11} using equations (2.59) and (2.60).

3.3.5 Applicable frequency bands and applications

The Republic of South Africa falls under the International Telecommunications Union (ITU) Region 1 and thus aligns its frequency allocations with those specified in the ITU Radio

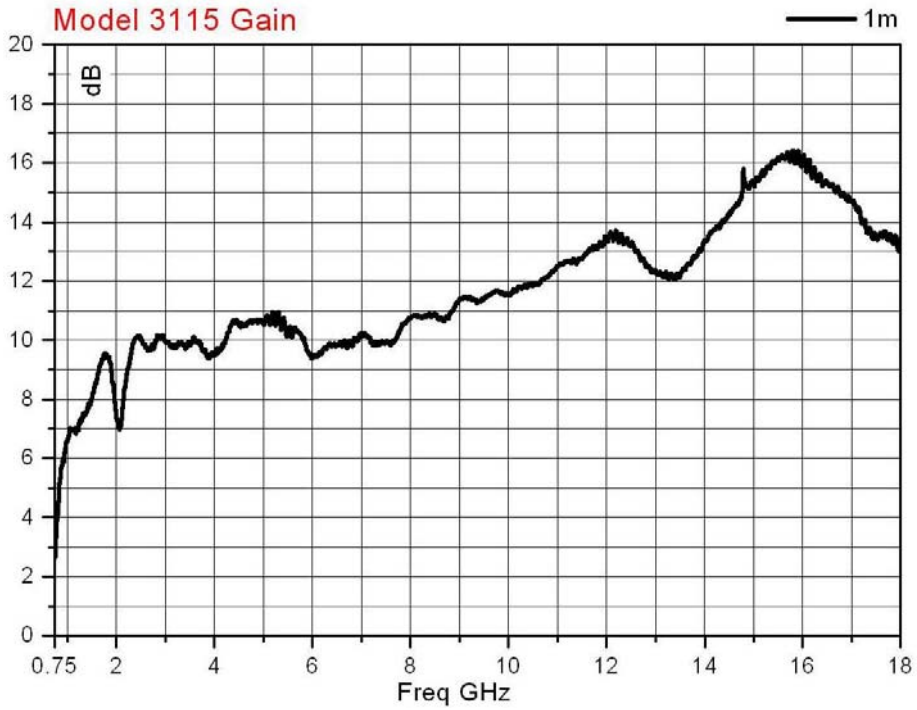

Figure 3.9: ETS-Lindgren antenna antenna-gain

Regulations as required by the Electronic Communications Act (ECA). The aim of the ECA is to promote convergence in the telecommunications, broadcasting and broadcasting signal distribution sectors and to provide the legal framework for the convergence of these sectors. The Independant Communications Authority of South Africa (ICASA) allocates frequency bands for primary and secondary services. Mobile communications and wireless network systems function in the UHF (300 MHz-3 GHz) and SHF (3 GHz-30 GHz) frequency bands. The ICASA allocations relevant to this research are listed in Table 3.3 [1]

The maximum theoretical radiated power allowed for GSM handsets is 1 W [85], and 100 mW [85] for wideband wireless systems such as WLAN and wideband data transmission applications. The maximum radiated power for broadband wireless access (WAS) is 200 mW [85]. With a signal to noise ratio (SNR) of less that 3 dB at the receiving device, the signal will become unintelligible. For effective SE, the SNR has to be decreased using an applied shield to less than 3 dB.

Frequency band	Application
790-890 MHz	fixed wireless links, UHF TV broadcast, wireless audio, security alarms, mobile wireless access, E-GSM cellular
890 MHz-1.215G Hz	fixed links, GSM cellular, distance measuring, surveillance radar, aeronautical radio navigation
1.215-1.429 GHz	radio navigation (GPS), space research, air traffic control radar, low capacity fixed links
1.300-1.525 GHz	fixed links, terrestrial digital audio broadcast, satellite digital audio broadcast
1.525-1.610 GHz	space operation, fixed links, mobile satellite, aeronautical navigation, GPS
1.610-1.660 GHz	mobile satellite, radio astronomy, space research, meteorological aids
1.660-1.710 GHz	mobile satellite, radio astronomy, space research, meteorological aids
1.710-2.170 GHz	fixed links, GSM1800, GSM1900, cordless phones,
2.170-2.520 GHz	fixed links, mobile satellite, WLAN, industrial scientific and medical (ISM), aeronautical video surveillance, broadband wireless access (WAS)
2.520-2.700 GHz	broadband WAS, space research, radio location, radio navigation

Table 3.3: ICASA frequency band allocations [1]

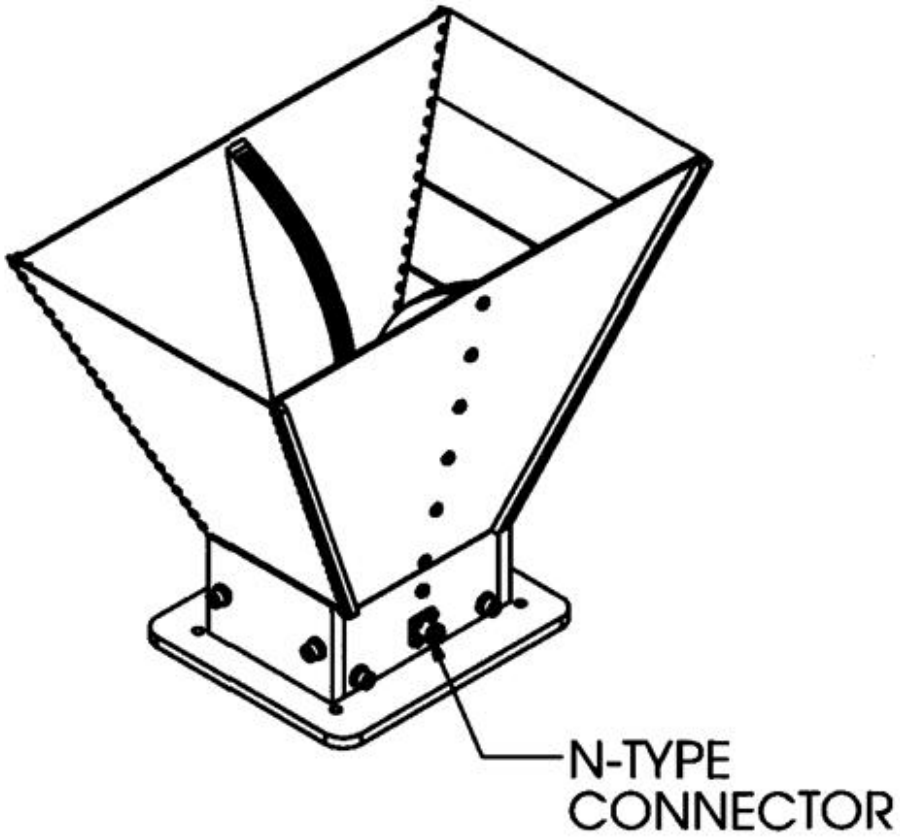

Figure 3.10: Saab-Grintek Technologies antenna used as transmitting antenna

3.4 DATA COLLECTION

The scattering parameters S_{11} and S_{21} were measured for the various samples using the setup in Figure 3.6. The performance of the samples in the mobile communication and WiFi frequency bands was investigated as indicated in Table (3.5). The prepared samples were labelled for identification purposes as indicated in Table (3.4). Wideband measurements of 800 MHz to 3 GHz were also done to cover the frequency bands assigned by ICASA in Table 3.3.

The result of each measurement was saved in a text file by the VNA and then processed with Microsoft Excel. The processed data was imported into Matlab and then presented graphically.

Sample Lable	Cement	Sand	EMD	CHY13K
0EMD	1	6	0	0
1EMD	1	5	1	0
2EMD	1	4	2	0
3EMD	1	3	3	0
4EMD	1	2	4	0
5EMD	1	1	5	0
3CHY13K	1	3	0	3
4CHY13K	1	2	0	4
5CHY13K	1	1	0	5

Table 3.4: Composite ratio of test samples

Band	Frequency (MHz)
GSM850	824 - 894
GSM900	890 - 960
GSM1800	1710 - 1880
GSM1900	1860 - 1990
WiFi	2400 - 2484

Table 3.5: Mobile communication and WiFi frequency bands

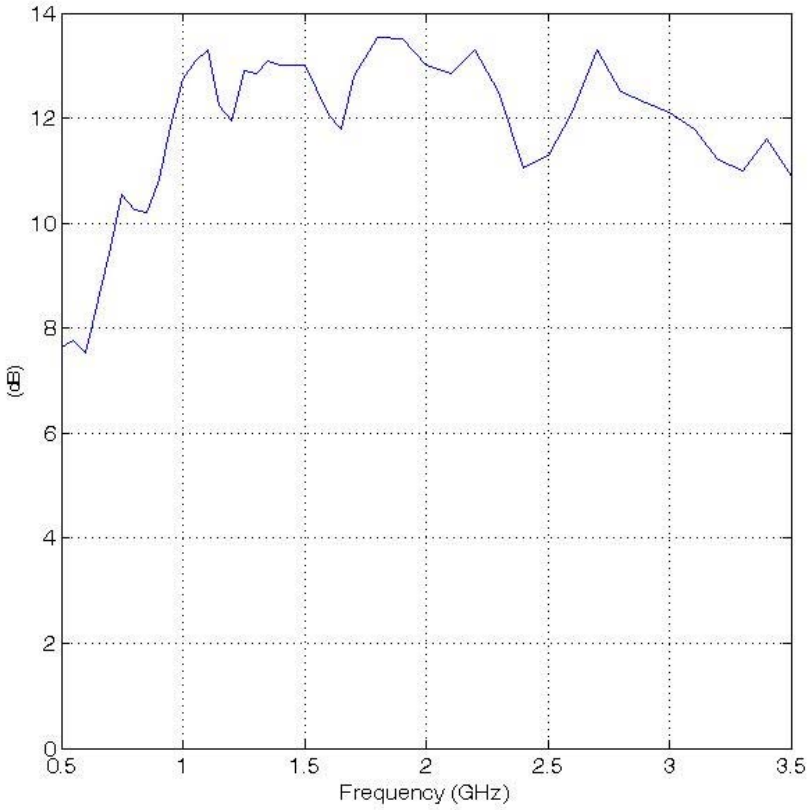

Figure 3.11: Antenna gain of the Saab-Grintek Technologies antenna used as transmitting antenna

3.5 CONCLUSION

In Chapter 3 various measuring techniques used in literature is discussed. The mathematical representation and transmission line model of shielding material is presented and simulations are done of the EMW SE of material with predetermined characteristics. The results of the simulations are compered with the measured results in Chapter 4.

The method followed to prepare the samples used for the research is explained. The magnetic and ferrimagnetic powder used is discussed. The required curing time of the samples is investigated and determined.

The implemented measuring system and equipment used are discussed and explained. An overview of the applicable frequency bands and applications are also given.

CHAPTER 4

RESULTS

The captured data of the various samples is displayed graphically and then discussed to highlight the findings of this reseach.

4.1 SHIELDING EFFECTIVENESS

The measured SE of the various samples is shown in Figures 4.1 to 4.9. The 0EMD sample is plaster cement as normally used in the building industry. The results in Figure 4.1 show losses below 3 dB in the GSM and WiFi frequency bands, which explains the good mobile communication reception in buildings. There is, however, an increase of SE above 5 dB between 1.2 and 1.5 GHz with a 7.4 dB peak at 1.36 GHz. This peak is also present in the other samples.

4.1.1 Shielding effectiveness of electrolyte manganese dioxide samples

Figures 4.2 to 4.5 show the measured results of the EMD samples. With an inclusion of 29%*vol* of manganese powder (EMD) as magnetic additive to the composite mixture, the 2EMD sample has an SE increase of 1 dB over the 800 MHz to 3 GHz measured frequency band, as indicated in Figure 4.2. The addition of the manganese powder also created a 8 dB peak at 1.2 GHz which was present in all the samples loaded with EMD. The 3EMD sample with 43%*vol* EMD powder shows a further SE increase in Figure 4.3.

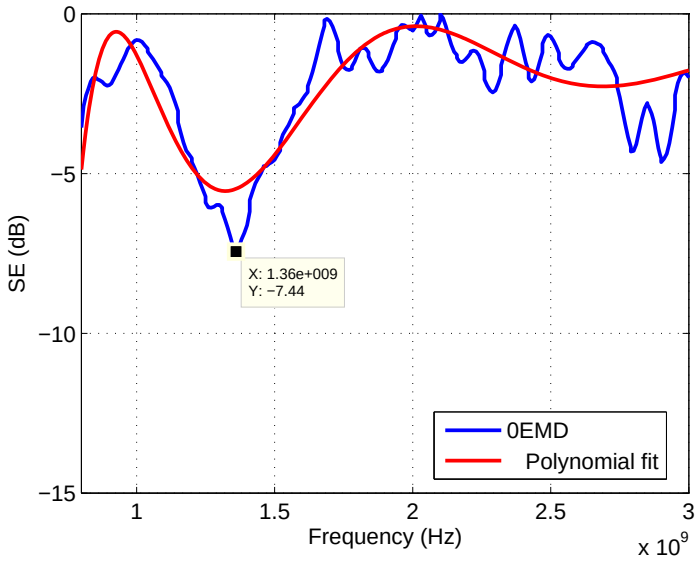

Figure 4.1: Measured SE of 0EMD sample (plaster cement)

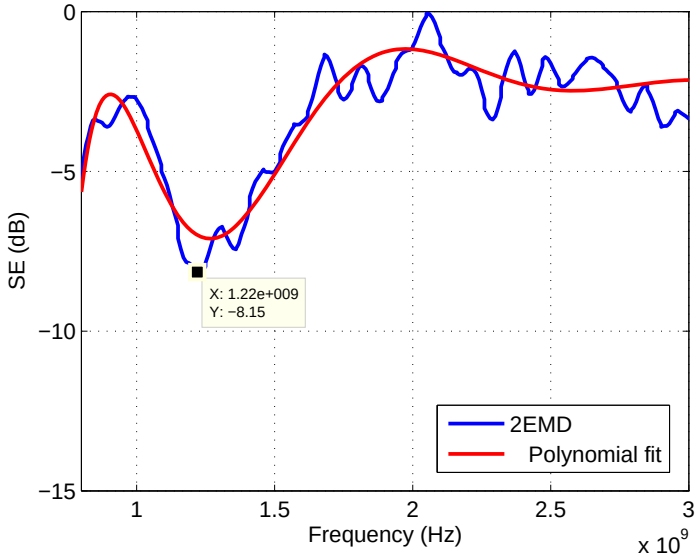

Figure 4.2: Measured SE of 2EMD sample

A significant improvement of SE resulting from the addition of 57%*vol* EMD (4EMD sample) is visible in Figure 4.4. The 5EMD sample with 71%*vol* EMD has an SE of more than 8*dB* in the GSM850 and GSM900 frequency bands, as shown in Figure 4.5. The magnetic powder also results in an SE peak of 2.9 GHz for all the tested samples and more than 70% signal reduction by the 5EMD sample. Table 4.1 shows a summary of the average and

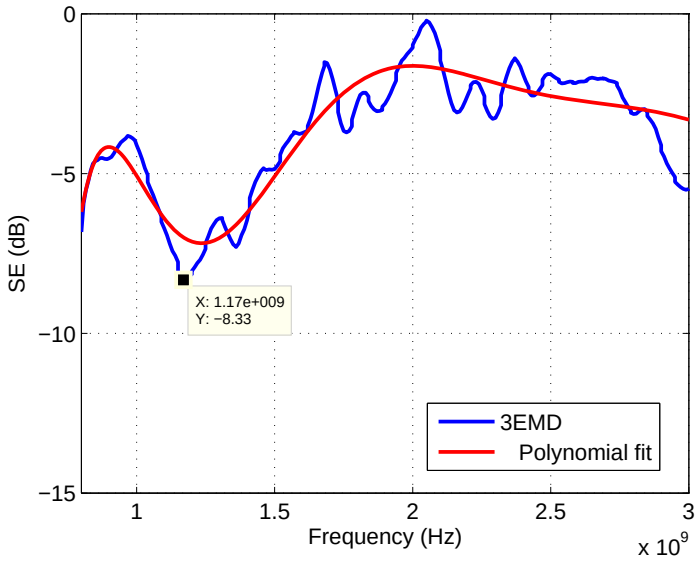

Figure 4.3: Measured SE of 3EMD sample

maximum SE measured for the EMD samples from 800 MHz to 3 GHz. The SE of the EMD samples has increased with 4 dB with the addition and increase of 71%*vol* EMD in the plaster cement.

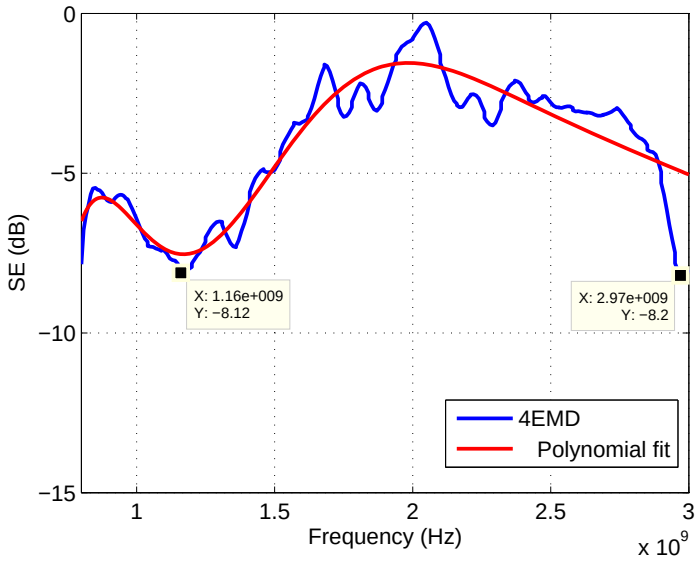

Figure 4.4: Measured SE of 4EMD sample

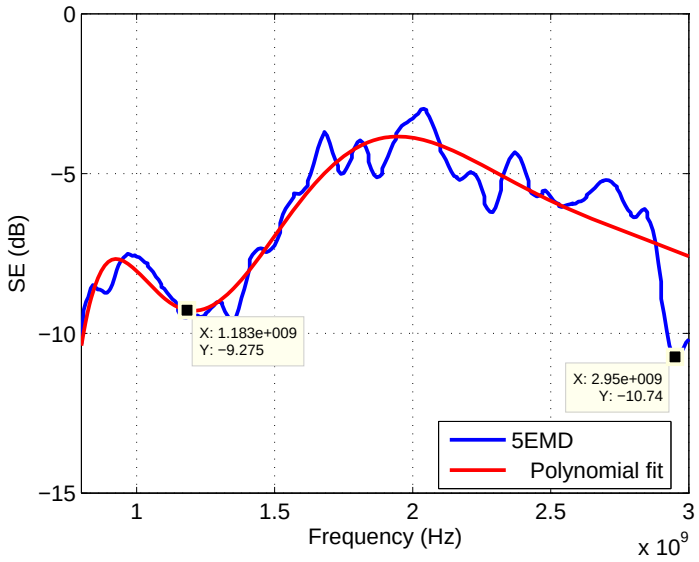

Figure 4.5: Measured SE of 5EMD sample

4.1.2 Shielding effectiveness of MnZn ferrite samples

The MnZn ferrite powder resulted in two peaks at 1.36 and 2.9 GHz but no significant SE improvement in the GSM and WiFi frequency bands. These results are shown in Figures 4.6 to 4.8. Table 4.2 shows a summary of the average and maximum SE measured for the CHY13 (MnZn ferrite) samples from 800 MHz to 3 GHz.

The SE improvement of plaster cement by increasing the %*vol* of EMD to the mixture is

Sample	Avg. SE	Max. SE
0EMD	-2 dB	-7.4 dB
2EMD	-3 dB	-8.2 dB
3EMD	-3.6 dB	-8.3 dB
4EMD	-4 dB	-8.2 dB
5EMD	-6.2 dB	-9.3 dB

Table 4.1: Summary of the average and maximum SE measured from 800 MHz to 3 GHz for the EMD samples

Sample	Avg. SE	Max. SE
3CHY13	-2.9dB	-8.9dB
4CHY13	-2.5dB	-9dB
5CHY13	-3dB	-9.6dB
2EMD3CHY13	-3.9dB	-8.8dB

Table 4.2: Summary of the average and maximum SE measured from 800 MHz to 3 GHz for the CHY13 samples

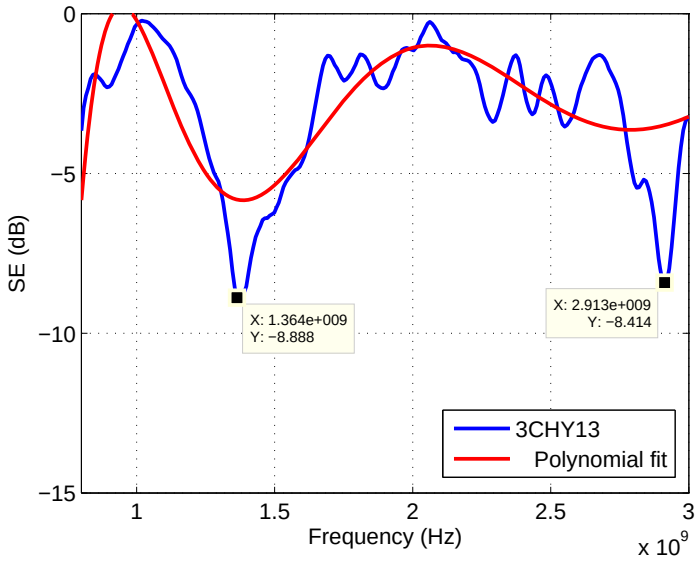

Figure 4.6: Measured SE of 3CHY13 sample

clearly visible in Figure 4.10, which shows a comparison of normal plaster cement and plaster cement with a 71%*vol* of EMD.

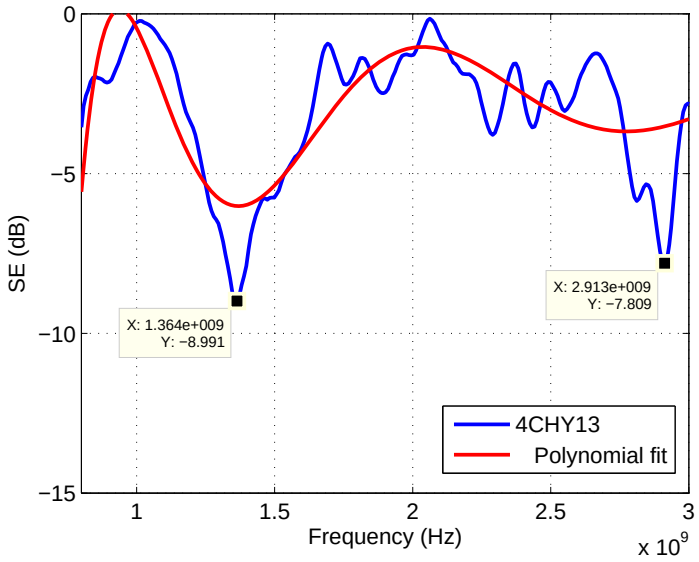

Figure 4.7: Measured SE of 4CHY13 sample

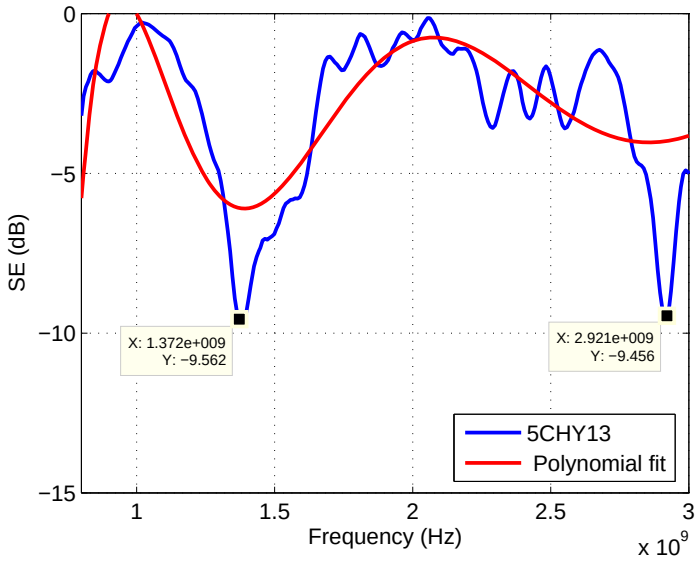

Figure 4.8: Measured SE of 5CHY13 sample

4.2 EFFECT OF MOISTURE CONTENT

The moisture content of the sample mixture has a large impact on the SE. Samples showed a stabilisation in SE only after 90 days of curing. The effect of the presence of moisture is shown in Figures 4.11 and 4.12 for normal plaster cement, and in Figures 4.13, 4.14, and

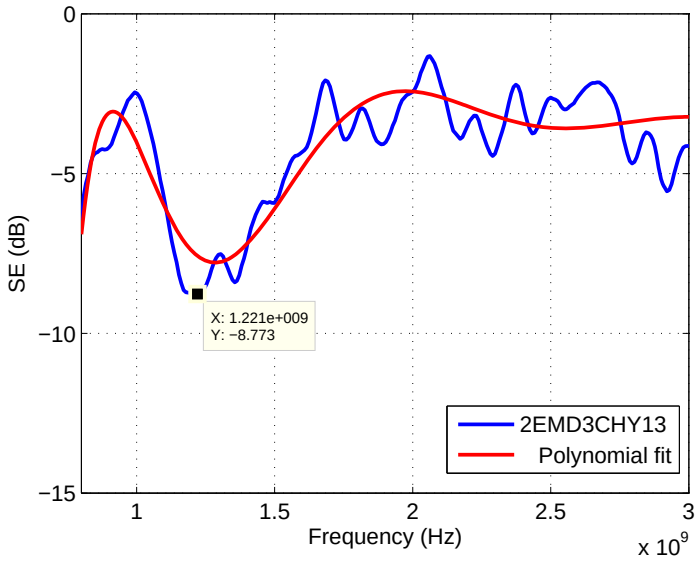

Figure 4.9: Measured SE of 2EMD3CHY13 sample

4.15 for the 5EMD sample.

The results indicated in Figures 4.13, 4.14, and 4.15, confirms the findings of [68], [73] and [75]. The results accepted as reliable were recorded after 120 days of curing and is shown in 4.14. The SE in the samples prior to the 120 days curing time, was mainly due to reflection loss because of the higher moisture content.

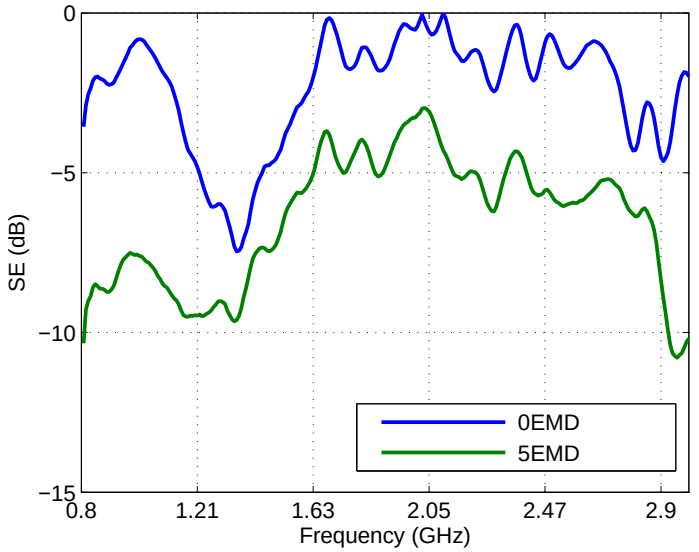

Figure 4.10: Increased SE with increased %vol of magnetic material

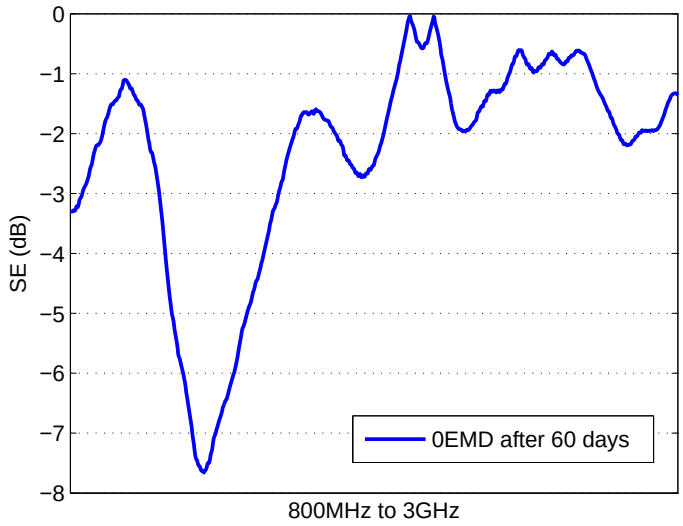

Figure 4.11: Measured SE of 0EMD sample after 60 days of curing

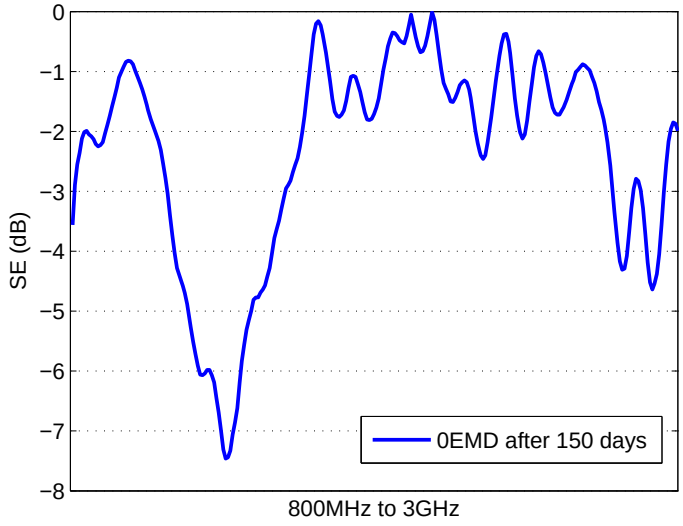

Figure 4.12: Measured SE of 0EMD sample after 150 days of curing

4.3 MEASURED REFLECTION AND ATTENUATION LOSS

Very low reflection loss is measured in the GSM850 and GSM900 frequency bands, confirming that the 5EMD sample has a high absorption capability for EMW. More than 80% of the incident EMW is absorbed by the sample. It should be noted that the measured attenuation

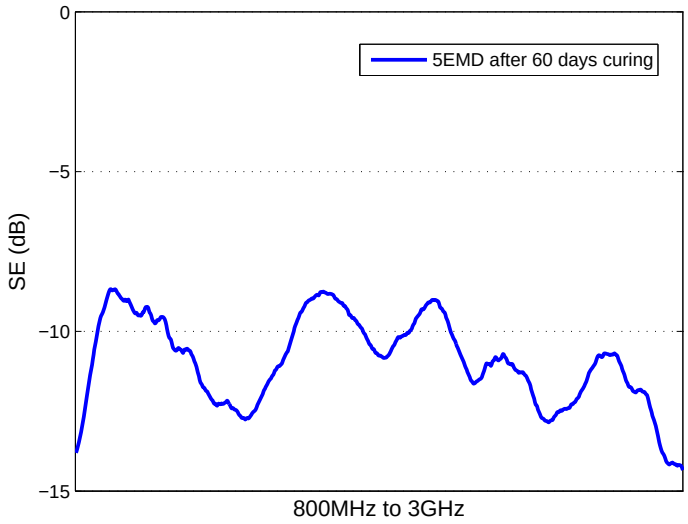

Figure 4.13: Measured SE of 5EMD sample after 60 days of curing

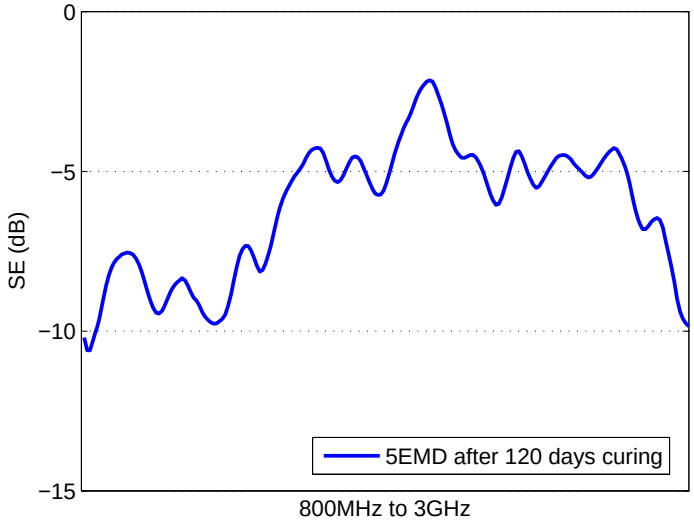

Figure 4.14: Measured SE of 5EMD sample after 120 days of curing

loss is the sum of attenuation and multiple internal reflection and attenuation losses. Figure 4.16 shows that the SE is mainly due to attenuation. In Figure 4.17 a very similar reflection loss in the GSM1800 and GSM1900 frequency bands but much lower SE indicates that the sample has high absorption but lower attenuation therefore resulting in the lower SE. Table 4.3 shows the average reflection, attenuation and transmission losses in the GSM frequency

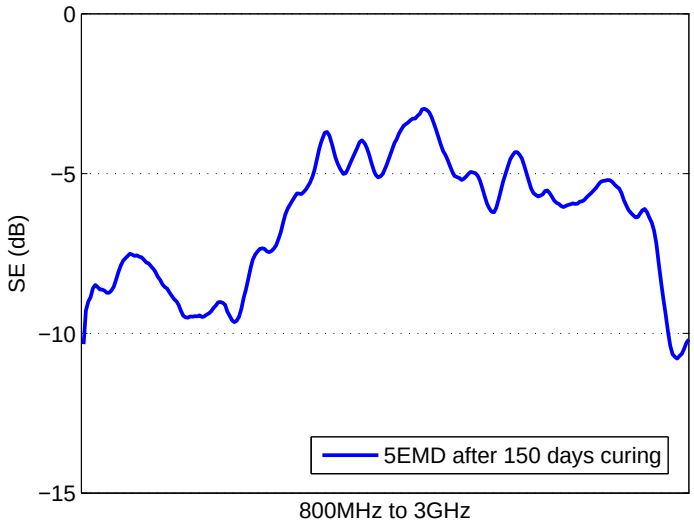

Figure 4.15: Measured SE of 5EMD sample after 150 days of curing

GSM band	Reflection loss	Attenuation loss	Transmission loss
GSM850 and GSM900	1.9 dB	6.5 dB	8.4 dB
GSM1800 and GSM1900	2 dB	2.4 dB	4.4 dB

Table 4.3: Summary of the average reflection, attenuation and transmission losses in the GSM bands for the 5EMD sample

bands for the 5EMD sample.

In the WiFi frequency band from 2.4 GHz and higher, the reflection loss is much greater with a peak of 8 dB reflection loss at 2.9 GHz, as can been seen in Figure 4.18, resulting in only 40% of the incident EMW being absorbed; consequently the SE is mainly due to reflection.

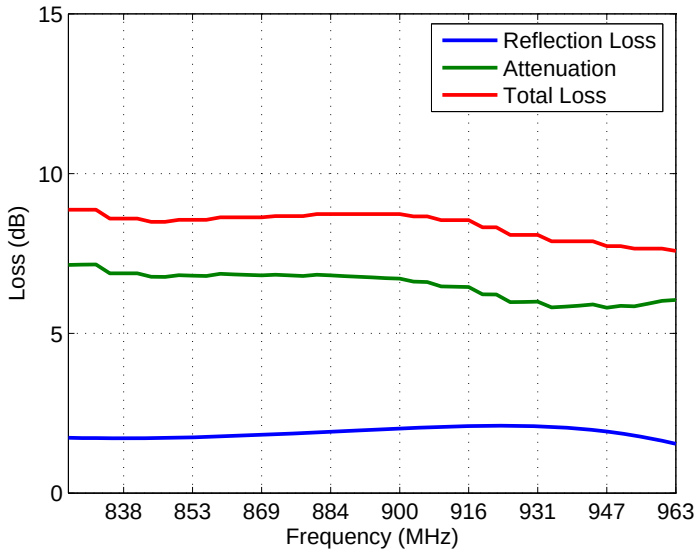

Figure 4.16: Measured reflection loss, attenuation and transmission loss in the GSM850 and GSM900 frequency bands for the 5EMD sample

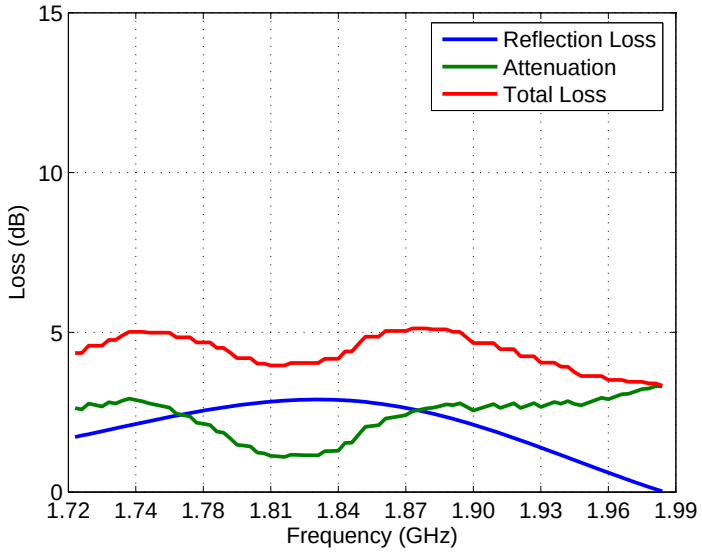

Figure 4.17: Measured reflection loss, attenuation and transmission loss in the GSM1800 and GSM1900 frequency bands for the 5EMD sample

4.4 COMPARISON OF MEASURED AND CALCULATED SE

Figure 4.19 compares the measured and calculated SE results. The polynomial fit of the measured SE shows a close comparison with the calculated SE. The measured reflection loss

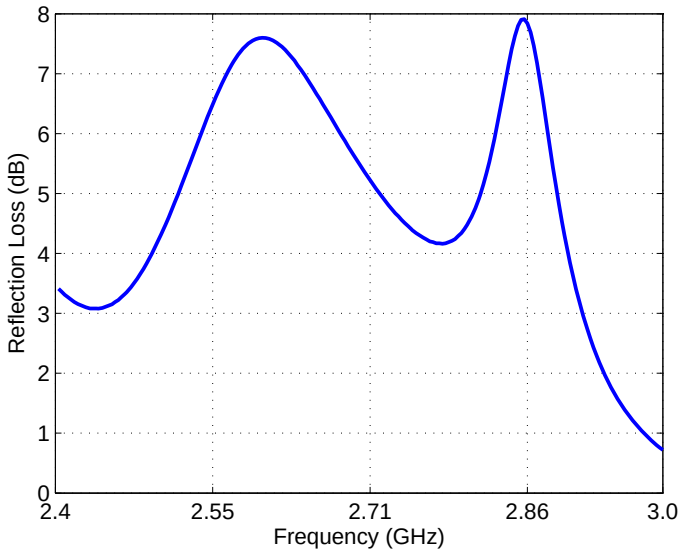

Figure 4.18: Measured reflection loss in 2.4 GHz to 3.0 GHz frequency band for the 5EMD sample

and attenuation in Figures 4.19 and 4.17 are also close in comparison with to the calculated results in Figure 4.19. The difference between the measured and simulated results is because of the uncertainty of the exact permeability, permittivity and conductivity values of the sample material.

4.5 CONCLUSION

Tables 4.1 and 4.2 shows that the increase of EMD content in the samples resulted in an average SE increase of 4.2 dB. The MnZn ferrite did not have the same effect as the EMD and only increased the SE by 2 dB for the same amount added to the composite mixture. The effect of moisture content on the SE is monitored over 150 days of curing and it was found that the SE only stabilised after 120 days. This finding confirms that determination of the SE in cement-based mixtures can only be done with proper curing.

The cement-based composite material with EMD as additive magnetic filler showed the best SE in the GSM850 and GSM900 frequency bands. Figure 4.19 shows that the sample has low reflection loss and high absorption with high attenuation inside the

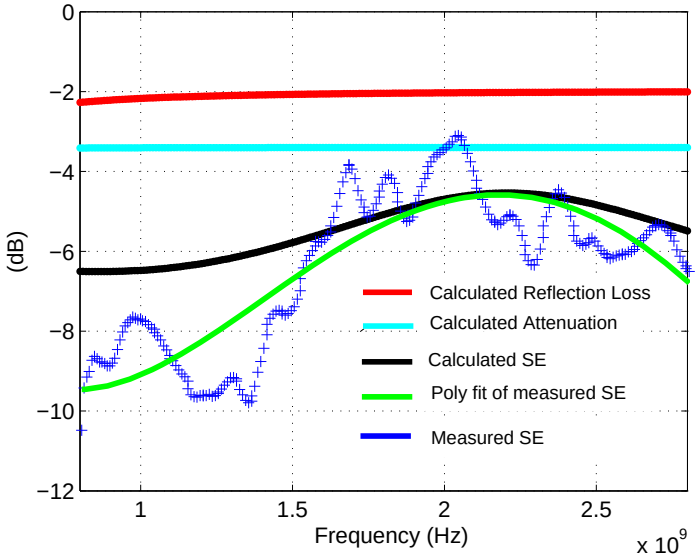

Figure 4.19: Comparison of measured and calculated SE for the 5EMD sample in the 800 MHz to 2.8 GHz frequency band

composite material. There is also a good comparison between the measured and calculated simulation values.

CHAPTER 5

CONCLUSION

5.1 SUMMARY

From the work described in this study, the following can be concluded:

5.1.1 Findings by this study

SE is a combined system of absorption, reflection and attenuation, and is a measure of the capability of the shielding material to reflect and attenuate an incident EMW. The complex permeability, permittivity and conductance of a material determine the magnitude of the SE. The uneven anti-parallel alignment of adjacent atomic spin magnetic moments in ferrimagnetic material increases its complex permeability.

To predict SE, the shielding material can be represented by a transmission line model. Plaster cement with no magnetic additive has high absorption, low reflection loss and low attenuation, resulting in a low SE. The mathematical simulation shows that the magnetic strength of an EMW propagated through the shielding material will be attenuated more by material with increased complex permeability. Increasing the %*vol* of magnetic material in the composite plaster cement improves the SE of the material. According to equation (2.85), if the thickness of the test sample is increased, the attenuation will increase, thus resulting in a higher SE. However, the thickness should be limited to ensure the practical implementation of the composite plaster cement.

The composite material needs to be well cured to ensure that the moisture content does not influence the measured results. Measured results only stabilised after 90 days of curing.

5.1.2 Contributions by this study

A measurement setup with the test sample inserted between the TX and RX antennae in an anechoic chamber provides accurate results. The scattering parameters were measured with a VNA and it was found that the reflection loss, absorption and attenuation can be accurately determined. The study shows that magnetic material can be mixed with plaster cement to produce a composite material that has increased complex permeability with improved SE.

MnO_2 and $MnZn$ ferrite were investigated as magnetic fillers and it was found that it can be used as magnetic material. MnO_2 resulted in a higher SE than $MnZn$ ferrite for the same $\%vol$ added to the plaster cement mixture.

5.2 RECOMMENDATIONS FOR FUTURE RESEARCH

Some recommendations for the extension of this work could be the following:

The SE of the shielding material may be improved by the addition of metal particles or carbon powder to increase reflection loss. This would however, decrease the absorption and attenuation of the shielding material. The SE may also be improved by the addition of 1 mm spherical EPS to increase the multiple internal reflections and attenuations [6].

Co-channel interference in indoor wireless communication systems can be successfully reduced by electromagnetic shielding to increase radio isolation between adjacent systems [86]. The composite plaster cement could be applied to the wall surface of the structure to achieve this goal. The strategy would be to identify the existing walls through which the interference propagates and subsequently shield them.

REFERENCES

[1] ICASA, "Draft south african table of frequency allocations," *Government Gazette*, pp. 3–188, July 2008.

[2] M. Jacob, T. Kurner, R. Geise, and R. Piesiewicz, "Reflection and transmission properties of building materials in *D*-band for modeling future mm-wave communication systems," in *Proc. 2010 IEEE 4th Euro. Conf. on Antennas and Propagation*, Barcelona, Spain, 12-16 April 2010.

[3] M. Badic and M.-J. Marinescu, "$SE\,(dB)$ determination for non-conductive electromagnetic absorbers," in *Proc. 2004 IEEE Intl. Symp. on Electromagnetic Compatibility*, Santa Clara, CA, 9-13 Aug. 2004, pp. 557–561.

[4] Bantsis, G. and Mavridou, S. and Sikalidis, C. and Betsiou, M. and Oikonomou, N. and Yioultsis, T., "Comparison of low cost shielding-absorbing cement paste building materials in *X*-band frequency range using a variety of wastes," *Ceramics International*, vol. 38, pp. 3683–3692, July 2012.

[5] H. Guan, S. Liu, Y. Duan, and J. Cheng, "Cement-based electromagnetic shielding and absorbing building materials," *Cement and Concrete Composites, Elsevier*, vol. 28, pp. 468–474, 26 Jan. 2006.

[6] H. Guan, S. Liu, Y. Duan, and Y. Zhao, "Investigation of the electromagnetic characteristics of cement-based composites filled with *EPS*," *Cement and Concrete Composites, Elsevier*, vol. 29, pp. 49–54, 6 Oct. 2007.

[7] R. Schulz, V. Plantz, and D. Brush, "Shielding theory and practice," *IEEE Trans. Electromagnetic Compatibility*, vol. 30, pp. 187–201, Aug. 1988.

[8] K.-Y. Park, S.-E. Lee, C.-G. Kim, and J.-H. Han, "Fabrication and electromagnetic characteristics of electromagnetic wave absorbing sandwich structures," *Composites Science and Technology, Elsevier*, vol. 66, pp. 576–584, 20 July 2006.

[9] H. Oka, K. Tanaka, H. Osada, K. Kubota, and F. Dawson, "Study of electromagnetic wave absorption characteristics and component parameters of laminated-type magnetic wood with stainless steel and ferrite powder for use as building materials," *Journal of Applied Physics*, vol. 105, pp. 07E701 – 07E701–3, 2009.

[10] A. Ogunsola, U. Reggiani, and L. Sandrolini, "Shielding effectiveness of concrete buildings," in *IEEE Int. Symp. Electromagnetic Compatibility and Electromagnetic Ecology*, Saint-Petersburg, 21-24 June 2005, pp. 65–68.

[11] H. Elkamchouchi and A. Abdelkader, "Evaluation of shielding effectiveness for different designs of building apertures in cellular communication frequency bands," in *Twenteith National Radio Science Conf.*, Cairo, Egypt, 18-20 March 2003.

[12] H. Lee and T. Yen, "Upgrading on cement-mortar properties for electromagnetic wave shielding in buildings," in *Proc. 2010 IEEE 2nd Intl. Conf. on Mechanical and Electronics Engineering*, vol. 1, 1-3 Aug. 2010, pp. 437–441.

[13] R. De Leo, G. Gradoni, A. Mazzoli, F. Moglie, G. Moriconi, and V. Primiani, "*DSP* cement composites for electromagnetic shielding: practice and experimental analysis," in *Proc. 2009 IEEE Intl. Symp. on Electromagnetic Compatibility*, Athens, Greece, 11-12 June 2009, pp. 1–4.

[14] D. Yawen, S. Mingqing, L. Chenguo, and L. Zhuoqiu, "Electromagnetic wave absorbing characteristics of carbon black cement-based composites," *Cement and Concrete Composites, Elsevier*, vol. 32, pp. 508–513, 1 April 2010.

[15] H. Oka, H. Hayakawa, H. Osada, A. Kano, H. Taniuchi, and O. Sawabe, "Laminated impregnated magnetic wood manufacturing methods and magnetic characteristics from dc to 13.5*GHz* band," *IEEE Trans. Magnetics*, vol. 38, pp. 3327–3328, Sep. 2002.

[16] K. Kimura and O. Hashimoto, "Three-layer wave absorber using common building material for wireless *LAN*," *Electronics Letters*, vol. 40, pp. 1323–1324, 25 Oct. 2004.

[17] G. Antonini, A. Orlandi, and S. D'elia, "Shielding effects of reinforced concrete structures to electromagnetic fields due to *GSM* and *UMTS* systems," *IEEE Trans. Magnetics*, vol. 39, pp. 1582–1585, May 2003.

[18] A. Ogunsola, U. Reggiani, and L. Sandrolini, "Shielding properties of conductive concrete against transient electromagnetic disturbances," in *IEEE Intl. Conf. Microwaves, Communications, Antennas and Electronics Systems*, Tel Aviv, 9-11 Nov. 2009, pp. 1–5.

[19] T. Yamane, S. Numata, T. Mizumoto, and Y. Naito, "Development of wide-band ferrite fin electromagnetic wave absorber panel for building wall," in *Proc. 2002 IEEE Intl. Symp. on Electromagnetic Compatibility*, vol. 2, Minneapolis, Minnesota, 19-23 Aug. 2002, pp. 799–804.

[20] J. Pretorius and B. Maharaj, "Ferrimagnetic composites in building material for electromagnetic wave absorption wireless communication systems," in *Proc. 2010 IEEE 4th Euro. Conf. on Antennas and Propagation*, Barcelona, Spain, 12-16 April 2010.

[21] Pretorius, J. and Maharaj, B., "Electrolytic manganese dioxide for *EMW* shielding effectiveness improvement of cement-based composites in indoor wireless communication systems," *International Journal of Physical Sciences*, vol. 8, pp. 295–301, Feb. 2013.

[22] P. Steffan, R. Vrba, and J. Drinovsky, "A new measuring method suitable for measuring shielding efficiency of composite material with carbon fibers," in *Proc. 2010 IEEE 5th Intl. Conf. on Systems*, Menuires, France, 11-16 April 2010, pp. 186–189.

[23] R. Oussaid, "Electromagnetic shielding effect of chiral and typical materials," in *Proc. 2008 Intl. Conf. on Computer Engineering and Systems*, Cairo, Egypt, 25-27 Nov. 2008, pp. 321–325.

[24] P. Jayasree, V. Baba, and B. Rao, "A case study on shielding effectiveness of laminated shields with conductive polymers," in *Proc. 2008 Intl. Conf. on Electromagnetic Interference and Compatibility*, Bangalore, India, 26-27 Nov. 2008, pp. 463–467.

[25] J. Sten and P. Koivisto, "Optimum transparent absorbers of electromagnetic waves," *IEEE Trans. Electromagnetic Compatibility*, vol. 50, pp. 1011–1014, Nov. 2008.

[26] M. Koledintseva, P. Ravva, J. Drewniak, A. Kitaitsev, and A. Shinko, "Engineering of ferrite-graphite composite media for microwave shields," in *Proc. 2006 IEEE Intl. Symp. on Electromagnetic Compatibility*, Portland, Oregon, USA, 14-18Aug. 2006, pp. 598–602.

[27] Y. Miyata and M. Matsumoto, "Thinner electromagnetic wave absorbers using ferroelectric substances," in *Proc. 1999 IEEE Intl. Symp. on Electromagnetic Compatibility*, Tokyo, Japan, 17-21 May 1999, pp. 416–419.

[28] Y. Nie, H. He, Z. Feng, and B. Xiong, "Absorbing properties of the magnetic composite electromagnetic wave absorber," in *IEEE Intl. Symp. on Microwave, Antenna, Propagation and Technologies for Wireless Communications*, Beijing, China, 8-12 Aug. 2005, pp. 724–727.

[29] T. Giannakopoulou, A. Kontogeorgakos, and G. Kordas, "Single-layer microwave absorbers: influence of dielectric and magnetic losses on the layer thickness," *Journal of Magnetism and Magnetic Materials*, vol. 263, pp. 173–181, Jan. 2003.

[30] Y. Song, D. Kim, C. Choi, and D. Lee, "Development of the *EM* wave absorber for *ETC* system using *MnZn*-ferrite and carbon," in *Microwave Conference*, Naha, Okinawa, Japan, 15-16 Nov. 2007, pp. 85–88.

[31] K. Hatakeyama and T. Inui, "Electromagnetic wave absorber using ferrite absorbing material dispersed with short metal fibers," *IEEE Transactions on Magnetics*, vol. 20, pp. 1261–1263, Sep. 1984.

[32] H. Oka, M. Terui, M. Osada, and Y. Izumida, F. Namizaki, "Controlling electromagnetic wave absorption characteristics by changing mixing ratios of magnetic powder of powder-type magnetic wood," in *IEEE Digests of Int. Magnetics Conf.*, Nagoya, Japan, 4-8 April 2005, p. 1099.

[33] E. da Silva, J. Rocha, P. Lins, S. da Nobrega, and M. de Alencar, "Characterization of electromagnetic radiation absorber materials," in *IEEE Intl. Conf. Microwave and Optoelectronics*, Brasilia, Brazil, 25-28 July 2005, pp. 326–329.

[34] P. Gornert, P. Payer, O. Surzhenko, L. Michalowsky, H. Heegn, E. Madai, and M. Langer, "Broad band electromagnetic absorption of flexible foils in the microwave range," in *Proc. 2007 IEEE Intl. Symp. on Electromagnetic Compatibility*, Honolulu, HI, 9-13 July 2007, pp. 1–5.

[35] R. Dosoudil, M. Usakova, J. Franek, A. Gruskova, and J. Slama, "Dispersion of complex permeability and EM-wave absorbing characteristics of polymer-based composites with dual ferrite filler," *Journal of Magnetism and Magnetic Materials*, vol. 320, pp. 849–852, May 2008.

[36] C. Beatrice, F. Fiorillo, F. Landgraf, V. Lazaro-Colan, S. Janasi, and J. Leicht, "Magnetic loss, permeability dispersion, and role of eddy currents in $Mn-Zn$ sintered ferrites," *Journal of Magnetism and Magnetic Materials*, vol. 320, pp. e865–e868, April 2008.

[37] Y. Li, C. Chen, S. Zhang, Y. Ni, and J. Huang, "Electrical conductivity and electromagnetic interference shielding characteristics of multiwalled carbon nanotube filled polyacrylate composite films," *Applied Surface Science, Elsevier*, vol. 254, pp. 5766–5771, 26 March 2008.

[38] N. Ishii, M. Miyakawa, and K. Sakai, "A method for achieving electromagnetic wave absorption by low-loss stratified construction materials," *IEEE Trans. Electromagnetic Compatibility*, vol. 47, pp. 105–111, Feb. 2005.

[39] R. Ramiz, "Shielding material for public buildings against the electromagnetic field radiation of the base station antennas," in *IEEE Topical Conf. Wireless Communication Technology*, Honolulu, HI, 15-17 Oct. 2003, pp. 475–476.

[40] F. Sagnard and G. El Zein, "Characterization of building materials for propagation modeling: frequency and time responses," *Intl. Journal Electronics and Communications, Elsevier*, vol. 59, pp. 337–347, 15 Sep. 2005.

[41] P. Paul, C. Christopoulos, and D. Thomas, "Time-domain simulation of electromagnetic wave propagation in saturating ferromagnetic materials," *Int. Journal of Numerical Modelling: Electronic Networks, Devices and Fields*, vol. 17, pp. 207–222, Jan. 2004.

[42] X. Chen and Y. Chen, "Time-domain test for material electromagnetic pulse shielding effectiveness based on shielding black-box windows method," in *Proc. 2012 Intl. Symp. on Electromagnetic Compatibility*, Shijiazhuang, China, 17-21 Sept. 2012, pp. 1–5.

[43] J. Shenhui, D. Ding, and J. Quanxing, "Measurement of electromagnetic properties of materials using transmission/reflection method in coaxial line," in *Asia-Pacific Conf. on Environmental Electromagnetics*, Hangzhou, China, 4-7 Nov. 2003, pp. 590–595.

[44] D. Ghodgaonkar, V. Varadan, and V. Varadan, "Free-space measurement of complex permittivity and complex permeability of magnetic materials at microwave frequencies," *IEEE Trans. on Instrumentation and Measurement*, vol. 39, pp. 387–394, April 1990.

[45] R. Pokharel, M. Toyota, and O. Hashimoto, "Analysis on effectiveness of wave absorbers to improve *DSRC* electromagnetic environment on express highway," *IEEE Trans. Microwave Theory and Techniques*, vol. 35, pp. 2726–2731, 1 Sept. 2005.

[46] C. Ropiak, M. McQuage, and W. Padilla-Vargas, "Electromagnetic field distribution as a function of building materials: Revisiting the standard definition of shielding effectiveness," in *Proc. 2009 IEEE Intl. Conf. on Electromagnetics in Advanced Applications*, Torino, Italy, 14-18 Sept. 2009, pp. 739–742.

[47] M. Romanca, P. Ogrulan, L. Aciu, and G. Nicolae, "Methods of investigating construction materials used for intelligent building shielding," in *Proc. 2008 IEEE Intl. Conf. on Optimization of Electrical and Electronic Equipment*, Brasov, Romania, 22-24 May 2008, pp. 191–196.

[48] T. Frenzel and M. Koch, "Modelling electromagnetic properties of typical building materials," in *Proc. 2008 IEEE Intl. Symp. on Electromagnetic Compatibility*, Hamburg, Germany, 8-12 Sept. 2008, pp. 1–6.

[49] T. Frenzel, M. Koch, and H. Garbe, "Determination of the transfer function of inhomogeneous shielding materials and implementation in an analytical model," in *Proc. 2009 IEEE Intl. Symp. on Electromagnetic Compatibility*, Athens, Greece, 11-12 June 2009, pp. 1–4.

[50] X. Zhang and W. Sun, "Microwave absorbing properties of double-layer cementitious composites containing *MnZn* ferrite," *Cement and Concrete Composites, Elsevier*, vol. 32, pp. 726–730, 17 July 2010.

[51] R. Leo, G. Gradoni, A. Mazzoli, F. Moglie, G. Moriconi, and V. Primiani, "*DSP* cement composites for electromagnetic shielding: practice and experimental analysis," in *Proc. 2007 IEEE Intl. Symp. EMC Europe Workshop Materials and Applications*, Athens, Greece, 11-12 June 2009, pp. 1–4.

[52] S. Hu, K. Tian, and Q. Ding, "Design and test of new cement based microwave absorbing materials," in *Proc. 2008 IEEE Intl. Symp. on Antennas, Propagation and Electromagnetic Theory*, Kunming, China, 2-5 Nov. 2008, pp. 956–959.

[53] R. Wilson, "Propagation through common building materials," University of Southern

California, Tech. Rep., Aug 2002, prepared for Magis Networks, Inc.

[54] A. Ogunsola, U. Reggiani, and L. Sandrolini, "Modeling shielding properties of concrete," in *Intl. Zurich Symp. on Electromagnetic Compatibility*, Singapore, 27 Feb. - 3 March 2006, pp. 34–37.

[55] Hutagalung, S.D. and Sahrol, N.H. and Ahmad, Z.A. and Ain, M.F. and Othman, M., "Effect of MnO_2 additive on the dielectric and electromagnetic interference shielding properties of sintered cement-based ceramics," *Ceramics International*, vol. 38, pp. 671–678, Jan. 2012.

[56] E. Unal, A. Gokcen, and Y. Kutlu, "Electromagnetic shielding," *IEEE Microwave Magazine*, vol. 6, pp. 48–54, August 2006.

[57] E. Savage, J. Gilbert, W. Radasky, and M. Madrid, "An alternative em shielding effectiveness measurement method for buildings," in *Asia-Pacific Intl. Symp. on Electromagnetic Compatibility*, Beijing, China, 12-16 April 2010, pp. 138–141.

[58] S. Razavi and M. Khalaj-Amirhosseini, "Optimum design of electromagnetic shielding rooms with minimum usage of absorbing materials," *Intl. Journal of RF and Microwave Computer-Aided Engineering*, vol. 20, pp. 22–32, Jan. 2010.

[59] G. Fei, Z. Bihua, G. Cheng, and C. Hailin, "Analysis of shielding effectiveness of conductive cement-based materials in hemp environment," in *Proc. 2008 Intl. Conf. on Microwave and Millimeter Wave Technology*, vol. 3, Nanjing, China, 21-24 April 2008, pp. 1460–1465.

[60] G. Fei and Z. Bihua, "Analysis of shielding effectiveness of monolayer and double layer cement shield rooms to hemp," in *Proc. 2008 China-Japan Joint Microwave Conference*, vol. 1, Shanghai, China, 10-12 Sept. 2008, pp. 505–508.

[61] D. Lee, K. Sowerby, and M. Neve, "Shielding strategies for interference mitigation in indoor wireless communications with frequency selective surfaces," in *Proc. 2005 Intl.*

Symp. on Antennas and Propagation Society, vol. 38, Washington DC, USA, 3-8 July 2005, pp. 260–263.

[62] W. Hayt Jr, *Engineering Electromagnetics*. McGraw-Hill, 1981.

[63] B. Pokharel and N. Karki, *Electrical Engineering Materials*. Narosa Publishing House PVT. LTD., 2007.

[64] H. Saadi and R. Oussaid, "Materials effect on shielding effectiveness," in *Proc. 2007 IEEE Intl. Conf. on Signal Processing and Communications*, Dubai, United Arab Emirates, 24-27 Nov 2007, pp. 999–1002.

[65] D. Svetanoff, W. Croisant, and N. Wehling, *IEEE Standard Method for Measuring the Effectiveness of Electromagnetic Shielding Enclosures*. IEEE, New York, USA, 28 Feb. 2007, vol. IEEE Std 299-2006.

[66] P. Bannister, "New theoretical expressions for predicting shielding effectiveness for the plane shield case," *IEEE Trans. Electromagnetic Compatibility*, vol. Proc. 2010 IEEE Intl. Symp. on Electromagnetic Compatibility, pp. 2–7, March 1968.

[67] X. Li, Q. Kang, and C. Zhou, "Research on absorbing properties of the concrete shielding material at 3*mmWave* bands," in *Proc. 2003 Asia-Pacific. Conf. on Environmental Electromagnetics*, Hangzhou, China, 4-7 Nov. 2003, pp. 536–540.

[68] S. Peer, K. E. Kurtis, and R. Zoughi, "Evaluation of microwave reflection properties of cyclically soaked mortar based on a semi-empirical electromagnetic model," *IEEE Trans. Instrumentation and Measurement*, pp. 2049–2060, 5 Oct. 2005.

[69] "Cement and concrete institude," http://www.cnci.org.za, last accessed: 2 Oct. 2012.

[70] H. Lee and T. Yen, "Upgrading on cement-mortar properties for electromagnetic wave shielding in buildings," in *Proc. 2010 Intl. Conf. on Mechanical and Electronics Engineering*, vol. 1, Kyoto, Japan, 1-3 Aug. 2010, pp. 437–441.

[71] L. Aciu, P. Ogrutan, and M. Badic, "New methods developed for shielding material characterization," *Annals of the Univ. of Craiova: Electrical Engineering*, vol. 33, pp. 1–4, 2009.

[72] "Weber," http://www.weber-tylon.co.za/plasters-decorative-finishes.html, last accessed: 2 Oct. 2012.

[73] S. Kharkovsky, M. F. Akay, U. Hasar, and C. Atis, "Measurement and monitoring of microwave reflection and transmission properties of cement-based specimens," *IEEE Trans. Instrumentation and Measurement*, vol. 51, pp. 1210–1218, 6 Dec. 2002.

[74] "Wikipedia," http://en.wikipedia.org/wiki/Portland-cement, last accessed: 2 Oct. 2012.

[75] U. Hasar, "A microcontroller-based microwave measurement system for permittivity determination of fresh cement-based materials," in *Proc. 2007 IEEE Intl. Instrumentation and Measurement Technology Conference*, Warsaw, Poland, 1-3 May 2007, pp. 1–6.

[76] M. Amano and Y. Kotsuka, "A method of effective use of ferrite for microwave absorber," *IEEE Trans. Microwave Theory and Techniques*, vol. 51, pp. 238–245, Jan. 2003.

[77] S. Fraia, M. Marracci, B. Tellini, and C. Zappacosta, "Shielding effectiveness measurements for ferromagnetic shields," *IEEE Trans. Instrumentation and Measurement*, vol. 58, pp. 115–121, Jan. 2009.

[78] L. Hatfield and B. Schilder, "Microwave shielding measurement method," in *IEEE Intl. Conf. Pulsed Power*, Washington, DC, 28 June-2 July 2009, pp. 1280–1284.

[79] A. Vasylchenko, V. Volski, W. De Raedt, and G. Vandenbosch, "Modelling of shielding effectiveness using small samples of tested materials," in *IEEE Intl. Conf. Mathematical Methods in Electromagnetic Theory*, Odesa, Ukraine, 29 June-2 July 2008, pp. 380–382.

[80] T. Tosaka, I. Nagano, S. Yagitani, and Y. Yoshimora, "Determining the relative permeability and conductivity of thin materials," *IEEE Trans. Electromagnetic Compatibility*, vol. 47, pp. 352–360, May. 2005.

[81] W. Fan, M. Panitz, S. Greedy, X. Ngu, and C. Christopoulos, "On the shielding effectiveness measurement of building materials at radio communication frequencies in reverberation chambers," in *Proc. 2010 IEEE Intl. Symp. on Electromagnetic Compatibility*, Beijing, China, 12-16 April 2010, pp. 1622–1625.

[82] J. Coder, J. Ladbury, and C. Holloway, "Using nested reverberation chambers to determine the shielding effectiveness of a material," in *Proc. 2007 IEEE Intl. Symp. on Electromagnetic Compatibility*, Honolulu, Hawaii, 9-13 July 2007, pp. 1–6.

[83] C. Holloway, D. Hill, J. Landbury, G. Koepke, and R. Garzia, "Shielding effectiveness measurements of materials using nested reverberation chambers," *IEEE Trans. Electromagnetic Compatibility*, vol. 45, pp. 350–356, May. 2003.

[84] I. Vilovic, N. Burum, and R. Nadj, "Estimation of dielectric constant of composite materials in buildings using reflected fields and *PSO* algorithm," in *Proc. 2010 IEEE 4th Euro. Conf. on Antennas and Propagation*, Barcelona, Spain, 12-16 April 2010, pp. 1–5.

[85] ICASA, "Regulations in respect of licence exemptions in terms of section 6 of the electronic communications act read with section 31(6) in respect of road frequency spectrum, electronic communicatins services and/or electronic communications network services," *Government Gazette*, pp. 3–13, April 2008.

[86] D. Lee, M. Neve, and K. Sowerby, "The impact of structural shielding on the performance of wireless systems in a single-floor office building," *IEEE Trans. Wireless Communications*, vol. 6, pp. 1787–1795, May 2007.